P62/SQSTM1 is a novel leucine-rich repeat kinase 2 (LRRK2) substrate that enhances neuronal toxicity

Kalogeropulou, Alexia F.; Zhao, Jing; Bolliger, Marc F.; Memou, Anna; Narasimha, Shreya; Molitor, Tyler P.

Published in:
Biochemical Journal

DOI:
10.1042/BCJ20170699

Publication date:
2018

Document Version
Peer reviewed version

p62/SQSTM1 is a novel Leucine Rich Repeat Kinase 2(LRRK2) substrate that enhances neuronal toxicity

Alexia F. Kalogeropulou[1,3], Jing Zhao[1], Marc F. Bolliger[1], Anna Memou[2], Shreya Narasimha[1], Tyler P. Molitor[1], William H. Wilson[1], Hardy J. Rideout[2] and R. Jeremy Nichols[1]*

[1]The Parkinson's Institute and Clinical Center, Sunnyvale, California USA.
[2]Division of Basic Neurosciences, Biomedical Research Foundation of the Academy of Athens, Athens, Greece.
[3]current address: MRC Protein Phosphorylation and Ubiquitylation Unit, University of Dundee, Dundee, UK.
*Correspondence and materials requests should be addressed to RJN (*jnichols@parkinsonsinstitute.org*).

This is the accepted manuscript version of Kalogeropulou, A. F., Zhao, J., Bolliger, M. F., Memou, A., Narasimha, S., Molitor, T. P., ... Jeremy Nichols, R. (2018). P62/SQSTM1 is a novel leucine-rich repeat kinase 2 (LRRK2) substrate that enhances neuronal toxicity. Biochemical Journal, 475(7), 1271-1293. DOI: 10.1042/BCJ20170699

Abstract

Autosomal dominant, missense mutations in the Leucine Rich Repeat protein Kinase 2 (*LRRK2*) gene are the most common genetic predisposition to develop Parkinson's disease (PD). LRRK2 kinase activity is increased in several pathogenic mutations [N1437H, R1441C/G/H, Y1699C, G2019S], implicating hyperphosphorylation of a substrate in the pathogenesis of disease. Identification of the downstream targets of LRRK2 is a crucial endeavor in the field to understand LRRK2 pathway dysfunction in disease. We have identified the signaling adapter protein p62/SQSTM1 as a novel endogenous interacting partner and substrate of LRRK2. Using mass spectrometry and phosphospecific antibodies, we found that LRRK2 phosphorylates p62 on Thr138 *in vitro* and in cells. We found that the pathogenic LRRK2 PD associated mutations [N1437H, R1441C/G/H, Y1699C, G2019S] increase phosphorylation of p62 similar to previously reported substrate Rab proteins. Notably we found that the pathogenic I2020T mutation, nor the risk factor mutation displayed decreased phosphorylation of p62. p62 phosphorylation by LRRK2 is blocked by treatment with selective LRRK2 inhibitors in cells. We also found that the amino terminus of LRRK2 is crucial for optimal phosphorylation of Rab7L1 and p62 in cells. LRRK2 phosphorylation of Thr138 is dependent on a p62 functional ubiquitin binding domain at its carboxy terminus. Co-expression of p62 with LRRK2 G2019S increases the neurotoxicity of this mutation in a manner dependent on Thr138. p62 is an additional novel substrate of LRRK2 that regulates its toxic biology, reveals novel signaling nodes and can be used as a pharmacodynamic marker for LRRK2 kinase activity.

Introduction

Parkinson's disease (PD) is a progressive neurodegenerative disorder with no known cure. PD is typically of idiopathic origin; however, it has been established that environmental exposures to toxins and inheritance of dominant or recessive mutations can precipitate the onset of disease. The neuropathological hallmark of Parkinson's disease is the presence of cytoplasmic alpha-synuclein inclusions (1,2). Cytoplasmic proteinaceous toxic aggregates are common features of multiple neurodegenerative disorders. Selective autophagy directs the clearance of aggregated proteins and dysfunctional organelles and it is thought that this process is necessary for handling these toxic aggregates. It is likely that autophagic handling of dysfunctional or aggregated proteins is disrupted in neurodegenerative diseases, and could be due to deregulation of protein chaperones or autophagy adapter proteins.

The adapter protein p62/sequestosome-1 (p62) is a component of cytoplasmic ubiquitin positive inclusions in PD and several protein aggregation based neurological disorders (3-11). The p62 protein has multiple characterized domains (12-14) including a PB1 domain (N'-Phos and Bem1 domain) that enables self-oligomerization and binds signaling molecules, an LC3 interaction region (LIR) and a ubiquitin binding domain (UBA) through which p62 binds ubiquitinated protein aggregates for sequestration and formation of the autophagosome. Other protein interaction domains are a TRAF6 binding domain (TB), nuclear import and export signals (NLS and NES), a KEAP interaction region (KIR) and a zinc finger domain (ZZ). p62 itself is an autophagy substrate and inhibition of autophagy machinery causes accumulation and oligomerization of p62 (15-17). The several functions and pathologies of p62 function are regulated by posttranslational modifications such as ubiquitination and phosphorylation (15,18). p62 activity bridges autophagy to the stress response pathway through regulation of the interaction of KEAP with Nrf2 to promote its stability and gene activation. This interaction is regulated by p62 phosphorylation at Ser349 by mammalian target of rapamycin complex 1 (mTORC1), Casein kinase 1 (CK1), and TAK1 (19-21). p62 facilitates the removal of intracellular organelles dependent on activation and phosphorylation by TBK1 on Ser403 (22,23). CK2 also regulates Ser403 increasing affinity for ubiquitin to regulate the selective clearance of ubiquitinated proteins (24). ULK1 phosphorylation of Ser407 regulates phosphorylation of Ser403 in an interplay of autophagy kinases (25). Additionally, p62 is phosphorylated by CDK1 at Thr269 (26), and p38δ phosphorylation of p62 Thr269 is necessary for amino acid dependent activation of mTORC1 (27). PB1 domain interaction partner selection can be regulated by phosphorylation by PKA on Ser24 (28).

Autosomal dominant, missense mutations in the Leucine Rich Repeat protein Kinase 2 (LRRK2) gene are a genetic predisposition to develop Parkinson's disease (PD) (29-33). LRRK2 mutations account for approximately 1-5% of familial and sporadic PD and are inherited with an autosomal dominant pattern with incomplete penetrance (34-39). The most common mutation leads to a serine substitution of Gly2019 in subdomain VII of the kinase domain (36), which increases kinase activity 2-4 fold (40-42). Other pathogenic inherited mutations in the Roc/COR domain (R1441G/C/H, Y1699C, and N1437H), also result in increased kinase activity, but are dephosphorylated at Ser910/935/955/973 (43). It is currently unknown how pathogenic mutations in LRRK2 across its multiple domains cause PD. Inhibition of LRRK2 kinase activity and several pathogenic LRRK2 mutations have been shown to alter LRRK2 protein complexes, with a dynamic loss and gain of binding partners, and redistribution within the cell.

Interestingly, cytoplasmic aggregates of LRRK2 expressed in cell culture and primary neurons co-localize with p62 (44,45). Further, over-expression of LRRK2 induces the accumulation of p62 (46,47), while LRRK2 knockouts similarly increase p62 accumulation (48,49), indicating a potential signaling axis for LRRK2 in regulating autophagy. LRRK2 has been associated with dysfunctions in multiple cellular processes (50) for example translation (51,52), mitochondrial health (53-56), vesicular trafficking and autophagy (45,57-66), cytoskeletal organization(67-72), WNT signaling (73,74), NFAT signaling (75) and inflammation.

Endogenous LRRK2 phosphorylation of a subset of Rabs implicates LRRK2 function in vesicular trafficking and autophagy (58). Several studies link LRRK2 function to autophagy, however the mechanism of how enhanced kinase activity, through mutation, alters protein degradation pathways has yet to be validated. However, LRRK2 kinase inhibition stimulates autophagy in several systems, implicating substrate modification in the process (76-78). Interestingly, it was reported that activated Nrf2 relieves some of the neuronal toxicity presented by overexpression of mutant LRRK2 (79), and p62 links autophagy and the Nrf pathway(19,80). In an attempt to identify a novel mechanism of LRRK2 function in stress response and autophagy, we investigated the functional interaction of LRRK2 with p62. We confirmed the interaction of LRRK2 and p62, and mapped the reciprocal sites of interaction in cells and *in vitro*. Proteins in complex with kinases are also sometimes substrates for these enzymes, and we found that p62 is phosphorylated by LRRK2 in a manner that depends on the LRRK2 amino terminus and phosphorylation on Ser910/935. LRRK2 [G2019S] neuronal toxicity is enhanced by co-expression with p62 in a manner dependent on Thr138. These data have important implications for the role of LRRK2 in neuronal stress response and death through the regulation of p62 (81).

Materials and Methods

Buffers, chemicals and antibodies.

Lysis Buffer contained 50 mM Tris/HCl, pH 7.4, 1 mM EGTA, 1 mM EDTA, 1 mM sodium orthovanadate, 10 mM sodium β-glycerolphosphate, 50 mM NaF, 5 mM sodium pyrophosphate, 0.27 M sucrose, 1 mM Benzamidine and 1 mM phenylmethanesulphonylfluoride (PMSF) and was supplemented with Sigma Protease Inhibitor Cocktail (Sigma) and ROCHE PhosStop (Roche). Detergents used in the lysis buffer are 1% Triton X-100 or 1% NP40. Lysis buffer used for endogenous p62/SQSTM1 pThr138 detection was supplemented with 0.15M NaCl and 0.5% NP40. Buffer A contained 50 mM Tris/HCl, pH 7.4, 50 mM NaCl, 0.1 mM EGTA and 0.27 M sucrose. Proximity Ligation Assay reagents were from Duolink. LRRK2 kinase inhibitor GNE1023 was described in (44) and synthesized at Genentech and provided by Genentech; PF475 was described in (82) and purchased from Sigma. Anti-GFP (clones 7.1 and 13.1) and anti-HA (clone 3F10) antibody are bought from Roche. Beta-actin (D6A8) and Hsp90 (C45G5) were from Cell Signaling Technologies. Anti LRRK2 (N241) is from Neuromab. Anti LRRK2 pSer935 (UDD2) and anti LRRK2 pSer1292 were from Abcam. Rabbit polyclonal anti-p62 phosphothreonine 138 antibody was generated by injection of the KLH conjugated phosphopeptide NGPVVGpTRYKC*SV (where pT is phosphothreonine and * indicates KLH conjugation site) into rabbits and was affinity purified by positive and negative selection against the phospho and de-phospho peptides respectively at Yenzym Inc. Anti phosphothreonine 138 was used at a final concentration of 1μg/mL in the presence of 10μg/mL non-phosphorylated peptide. Mouse anti-p62 (M162-3), rabbit anti-p62 (PM045), and rat anti-phospho-p62 Ser403 (D343-3) are from MBL. FLAG M2 antibody was purchased from Sigma. Mouse anti-β3 tubulin (Tuj1) was from Biolegend (Covance). Rabbit anti-active caspase-3 was from R&D Systems. Sheep anti-phospho Rab8, sheep anti-phospho Rab10, and sheep anti-phospho Rab7L1 were kind gifts from Professor Dario Alessi (MRC-PPU, University of Dundee, Scotland). Anti-GFP for immunoblotting was from Roche (clones 7.1 and 13.1) or rabbit monoclonal anti-GFP from LifeTechnologies was used for PLA. GFP-Trap Agarose was purchased from Chromotek. Calyculin A and Okadaic acid were from LC Labs, and MLi-2 (83) was a kind gift of Professor Dario Alessi (MRC-PPU, University of Dundee, Scotland).

Cell culture, treatments and cell lysis

Tissue culture reagents were from Life Technologies or Thermo Scientific. HEK-293 cells (from ATCC) were cultured in Dulbecco's Modified Eagle's medium supplemented with 10% FBS, 2mM glutamine and 1×antimycotic/antibiotic solution. The Flp-in T-REx system was

from Invitrogen and stable cell lines were generated as per manufacturer instructions by selection with hygromycin as has been described previously (Nichols et al., 2010;Doggett et al., 2012). T-REx cell lines were cultured in DMEM supplemented with 10% FBS and 2mM glutamine, 1X antimycotic/antibiotic and 15 µg/ml Blasticidin and 100 µg/ml hygromycin. The treatments were added as indicated time and concentration. Human lung alveolar epithelial A549 cells (from ATCC) were cultured in DME/F-12 with L-Glutamine and 10% FBS, 1x antimycotic/antibiotic. Human control lymphoblasts were a kind gift of Dr. Birgitt Schuele (The Parkinson's Institute, Sunnyvale CA) and cultured in RPMI supplemented with L-glutamine and 10%FBS, 1x antimycotic/antibiotic and 1x non-essential amino acid (Gibco). Mouse embryonic fibroblasts (MEFs) were cultured in DMEM supplemented with L-glutamine and 10%FBS, 1x antimycotic/antibiotic and 1x non-essential amino acid (Gibco). HEK293 and T-REx were transfected by the polyethylenimine method (84) and were lysed 48 hours after transfection. T-REx cultures were induced to express the indicated protein by inclusion of 1 µg/ml doxycycline in the culture medium for 48 hours. After the indicated culture conditions, cell lysates were prepared by washing once with PBS and lysing in situ with 0.4 ml of lysis buffer per 10cm dish on ice, then centrifuged at 15,000 x g at 4 °C for 15 minutes. Protein concentrations were determined using the Bradford method with BSA as the standard. *Generation and culture of CRISPR/Cas9 GFP-LRRK2 H1299 cells can be found in the* ***Supplemental Figure 1****.*

DNA Constructs

Restriction enzyme digests, DNA ligations and other recombinant DNA procedures were performed using standard protocols with Fermentas enzymes. DNA constructs used for transfection were purified from Escherichia coli DH5α using Qiagen plasmid Maxi kits according to the manufacturer's protocol. The pcDNA5-Frt-FLAG-LRRK2 and pcDNA5-Frt-GFP LRRK2 constructs, and pcDNA5-Frt-FLAG-LRRK1 used for transfections were provided by Professor Dario Alessi (MRC-PPU, University of Dundee, Scotland). The LRRK2 cDNA was sub-cloned from pcDNA3.1 (Melachroinou et al., 2016) into the pcms-EGFP reporter plasmid, expressing un-tagged LRRK2 and EGFP under separate promoters; or, into pcDNA3.1 with a C-terminal c-myc epitope tag. A plasmid encoding HA-tagged p62 was obtained from Addgene (plasmid #28027) and was subcloned into pcDNA5-Frt-FLAG and pGEX6P. pFLAG HDAC4 was a gift from Eric Verdin (Addgene plasmid #13821), pcDNA3 IKKε FLAG was a gift from Tom Maniatis (Addgene plasmid #26201), HDAC6 Flag was a gift from Eric Verdin (Addgene plasmid #13823), Harm Kampinga provided pcDNA5/FRT/TO-V5 HSPA1A (Addgene plasmid #19510), pcDNA5/FRT/TO-V5 HSPH1 (Addgene plasmid #19506) pcDNA5/FRT/TO-V5 HSPA8 (Addgene plasmid #19514), pcDNA5/FRT/TO-V5 DNAJB6b (Addgene plasmid #19528), pcDNA5/FRT/TO-V5 DNAJB1 (Addgene plasmid #63102) and pcDNA5/FRT/TO-V5 DNAJB8 (Addgene plasmid #19531). Hsp90 was a gift from William Sessa (Addgene plasmid #22487), pcDNA5-Frt-GFP-Rab7L1 was synthesized using codon optimization by GeneArt (ThermoScientific). DNA manipulations were carried out using standard techniques and mutagenesis was performed with the GeneArt mutagenesis kit (ThermoScientific).

Immunoprecipitation Assays

For transfected HEK293 or T-REx cells, cell lysates were prepared in Lysis buffer (0.4ml per 10cm dish) and subjected to immunoprecipitation with anti-FLAG M2 agarose or GFP-Trap A beads (Chromotek) at 4°C for 2 hours. Beads were washed twice with Lysis Buffer supplemented with 300mM NaCl, then twice with Buffer A. Immune complexes were incubated at 70°C for 10 minutes in LDS sample buffer, passed through a Spin-X column (Corning) to separate the eluate from the beads, then boiled. Equal amounts of immunoprecipitated protein were subjected to western blots with indicated antibodies. For endogenous LRRK2 immunoprecipitation, mouse anti-LRRK2 (N241; Neuromab) non-covalently conjugated to protein-G agarose (1µg antibody: 1µL bead) was used to enrich LRRK2 protein complexes from

A549 cells. Endogenous p62/SQSTM1 was immunoprecipitated by mouse anti-p62 (MBL) from human lymphoblastoid cells covalently conjugated to protein-A sepharose (1µg antibody: 1µL bead; Perce Crosslink IP Kit, ThermoScientific) and incubated at 4°C for 4 hours. The immunoprecipitated samples were analyzed by immunoblotting.

Protein Purifications

To induce the expression of GST-p62, *E. coli* BL21 Rosetta transformants of pGEX-6P plasmids harboring p62 or mutant p62 were grown to a OD_{600} of 0.5 at 37°C and induced at 30°C for 3 hours by the addition of IPTG (isopropylβ-D-thiogalactoside) to a final concentration of 1 mM. Cells were lysed by sonication in lysis buffer with 1% (v/v) Triton X-100 and 0.1% beta-mercaptoethanol. The soluble fraction was retrieved by centrifugation at 15000 g for 15 min. Recombinant protein was purified by glutathione–Sepharose chromatography, and proteins were eluted in buffer A with 20 mM glutathione, 1 mM benzamidine and 2 mM PMSF, or were liberated from the GST fusion by incubation with 0.1mg of precision protease per 1mg of protein.

Kinase assays

For assays using recombinant proteins as substrates, the reactions were set up in a total volume of 25 µl with recombinant kinase (GST-LRRK2$^{970-2527}$ or FLAG-LRRK2$^{1-2527}$) in 50mM Tris pH 7.5, 0.1mM EGTA, 10 mM $MgCl_2$ and 0.1 mM [γ-^{32}P] ATP (~500cpm/pmol), with p62 substrate, with the indicated concentrations of enzyme and substrate. After incubation for 30 min at 30°C, the reactions were stopped by the addition of Laemelli sample buffer. Reaction products were resolved by electrophoresis on NuPage Bis-Tris gels and stained with coomassie blue. The incorporation of phosphate into protein substrates was determined by autoradiography and/or immunoblotting with phosphospecific antibodies. Kinase reactions for mass spectrometry based phosphosite identification were carried out under similar conditions but with 200mM cold ATP and reactions were resolved by electrophoresis on NuPage Bis-Tris gels and stained with colloidal blue and p62 was excised and submitted for MS analysis at MS Bioworks.

Mass spectrometry

Sample Preparation and LC/MS/MS. Replicate gel segments were reduced using dithiothreitol, alkylated with iodoacetamide and then subjected to digestion with trypsin, chymotrypsin and elastase (Promega, Madison, WI). Digests were analyzed by nano LC/MS/MS with a NanoAcquity HPLC system (Waters, MA) interfaced to a Q Exactive tandem mass spectrometer (ThermoFisher, San Jose, CA). Peptides were loaded on a trapping column and eluted over a 75µm analytical column at 350nL/min; both columns were packed with Jupiter Proteo resin (Phenomenex, Torrance, CA). A 30 min gradient was employed for each digest. The mass spectrometer was operated in data-dependent mode, with MS and MS/MS performed in the Orbitrap at 70,000 and 17,500FWHM resolution, respectively. The fifteen most abundant ions were selected for MS/MS from each MS scan. Dynamic exclusion and repeat settings ensured each ion was selected only once and excluded for 30s thereafter.

Database searching. Product ion data were searched against the combined forward and reverse protein database using a locally stored copy of the Mascot search engine v2.5 (Matrix Science, London, U.K.) via Mascot Daemon v2.5. Peak lists were generated using Proteome Discoverer v1.4 (ThermoFisher). The database was appended with common background proteins. Search parameters were precursor mass tolerance 10 ppm, product ion mass tolerance 0.02 Da, 2 missed cleavages allowed, fully tryptic peptides only for trypsin and no enzyme specificity for chymotrypsin and elastase, fixed modification of carbamidomethyl cysteine, variable

modifications of oxidized methionine, protein N-terminal acetylation, pyro-glutamic acid on N-terminal glutamine and phosphorylation on serine, threonine and tyrosine.

Data Analysis. Mascot search result flat files (DAT) were parsed to the Scaffold software v3.1 (Proteome Software, Portland, OR) to create a non-redundant list per sample. The criteria for accepting a protein identification were determined by calculating the false discovery rates (FDR) from the concatenated forward/reverse database. This resulted in the following cutoff values: 90% protein and 50% peptide level probability (probabilities were assigned by the Protein Prophet algorithm), and a minimum of two unique peptides per protein. These criteria resulted in FDR of less than 1% at the protein level.

Immunocytochemistry and Proximity Ligation Assay (PLA)

For immunocytochemistry, cells were grown on coverslips and washed with PBS and fixed with 4% paraformaldehyde for 15 min, followed by two wash steps with PBS. After permeabilization for 5 min with PBST, a 30 min blocking step with 10% goat serum (Dako cytomation) in PBS was performed. This was followed by 2 hrs incubation with FLAG M2 antibody in PBS. After three washes with PBS for 5 min, the cells were incubated for 1 h with secondary antibody (Alexa Fluor® -conjugated antibody, 1:500 dilution, Molecular Probes) and washed three times for 5 min with PBS. PLAs were performed on eight-well CC2 chamber slides. Cells were fixed and permeabilized as in the immunocytochemistry experiments, then blocked with Duolink Blocking Solution for 30 min at 37 ◦C. Immediately after blocking, the cells were incubated with the indicated primary antibodies in the Duolink Antibody Diluent for 1 h at room temperature (20–24 ◦C). The cells were washed twice with Duolink Wash Buffer A for 5 min before the incubation of the PLUS and MINUS PLA probes. The cells were incubated with PLA probes for 1 h at 37 ◦C, followed by two washes with Wash Buffer A for 5 min. The cells were then incubated with pre-mixed Ligation-Ligase solution at 37 ◦C for 30 min. After two washes with Wash Buffer A for 2 min, the cells were incubated with pre-mixed Amplification-Polymerase solution for 60–90 min at 37 ◦C. Finally, the cells were washed twice with Duolink Wash Buffer B for 10 min, followed by 0.01 × Wash Buffer B for 1min. The slides were dried in the dark and mounted with Duolink II Mounting Medium. The images were taken by Nikon Eclipse TI florescence microscope and quantified by Duolink ImageTool (Version 1.0.1.2), around 150 cells signal were counted for each sample. The quantification data was graphed by Prism5 (GraphPad), and statistics was calculated by one way ANOVAs. The quantification of the PLA results was from 3 independent experiments.

Primary Neuronal Survival Assays

Primary rat embryonic cortical neurons were prepared as described (Melachroinou et al., 2016). Briefly, embryonic day 17 rat cortices were dissociated in trypsin/DNAse followed by gentle mechanical disruption. Dissociated neurons were plated at a density of approximately 125,000 cells per cm^2 in complete Neurobasal medium with l-glutamine, penicillin/streptomycin, and B-27 serum free supplements (all components from Thermo Scientific). On day four following plating, the neurons were transiently transfected with un-tagged human LRRK2 (WT or G2019S) cDNA in pcms-EGFP expression vector using Lipofectamine 2000 (Thermo Scientific) as described previously (85), together with FLAG-tagged p62 (WT or T138A) at a ratio of 3:1 with LRRK2 in excess. Three days following transfection, the neurons were fixed in 4% paraformaldehyde, and processed for anti-LRRK2 (MJFF c41-2) or anti-FLAG/anti-GFP immunofluorescence, with DAPI as a nuclear counterstain. Co-expression of p62 and LRRK2 within individual neurons, transfected with an excess of LRRK2 cDNA, was confirmed by co-immunostaining for anti-Flag and anti-LRRK2 (clone c41-2); and the neuronal phenotype of the cultures was established by triple immunostaining for anti-GFP, anti-Flag, and anti-β3 tubulin. The stained coverslips were observed under 40X magnification, and neurons double positive for EGFP and FLAG were

scored according to their nuclear morphology. Neurons were considered to be apoptotic if two or more condensed chromatin bodies were observed within a neuronal profile. From at least four parallel coverslips (performed from 2 independent cultures), 100 positive neurons were counted by a researcher blind to the experimental conditions, and apoptotic neurons were expressed as a percentage of neurons positive for both FLAG and EGFP. Parallel coverslips were co-immunostained for anti-Flag and anti-active caspase-3, together with DAPI, as an additional marker of neurons undergoing apoptotic cell death.

Results

LRRK2 interacts with p62

LRRK2 is known to interact with chaperone proteins Hsp90, Cdc37, Hsp70 and Hsc70 (64,86-88). These chaperones are necessary for proper folding of proteins. Since cytoplasmic accumulations of LRRK2 have been found coincident with p62, we sought to survey several protein chaperones involved in post-translational protein handling. Using epitope tag immunoprecipitations we screened a panel of protein chaperones for interaction with LRRK2 using plasmid based expression in T-REx 293-GFP or T-REx 293-GFP-LRRK2 cells. We tested the signaling chaperone Hsp27, along with the protein folding chaperones DNAJB6 (Hsp40), DNAJB8 (Hsp40), HSPA1A (Hsp70), HspA8 (Hsc70), Hsp90, HSPH1 (Hsp110), and also HDAC6 and p62 which are autophagy related proteins that can shuttle cargo to aggresomes or autophagosomes. We found that LRRK2 interacts with all of these chaperones in this expression system, as well as p62 and HDAC6, except for Hsp110, **Figure 1A**. To determine spatial proximity of LRRK2 and p62 in cells, we performed the in situ Proximity Ligation Assay [PLA] on cells expressing GFP-LRRK2 and FLAG-p62, **Supp. Figure 2A**. We compared the number of signals per p62/LRRK2 co-transfected cell to the number of signals per cell transfected with cytoplasmic HDAC4 or vector alone and found a significant and specific increase in p62-LRRK2 signals (representative micrographs in **Supp. Figure 2A and B**). LRRK2 and its paralog LRRK1 harbor similar domain structure, and both could therefore interact with p62. We asked if p62 could interact with LRRK2 or LRRK1 in co-expression analyses. FLAG-tagged LRRK2 or LRRK1 were expressed with HA-p62, and anti-FLAG immunoprecipitates were analyzed for the presence of p62. LRRK1 has also been associated with autophagy, (89). **Figure 1B** shows that only p62 was highly enriched in LRRK2 immune-complexes, with a slight increase in the presence of LRRK2 inhibitor GNE1023.

We next sought to isolate endogenous LRRK2/p62 complexes. To do this, we tested two cell lines and immunoprecipitation methods. We first immunoprecipitated endogenous LRRK2 immunoprecipitates from A549 cells and found endogenous p62 present, **Figure 1C,** where inclusion of LRRK2 inhibitor resulted in a slight increase in the levels of p62 in the immunoprecipitate. Since we observed slight increases in p62-LRRK2 complexes in cells after LRRK2 inhibition, we sought to quantitate this interaction with the selective inhibitor MLi2 and found a reproducible, but modest increase in p62 co-precipitation with inhibited LRRK2, **Supp. Figure 2C**. We next employed the PLA on A549 cells to ask if endogenous LRRK2 and p62 were in close spatial proximity. Using specific antibodies against LRRK2 and p62, we found significant numbers of PLA signals for LRRK2/p62 complexes over IgG controls and significantly more PLA signals when treated with LRRK2 inhibitor for 90min, **Supp. Figure 2D**. To complement our endogenous interaction data with another immunological retrieval tool, We next expressed amino-terminal tagged GFP-LRRK2 from a Bacmam virus and 24 hours after infection cells were fixed at 0, 30min and 3hrs after treatment with LRRK2 inhibitor, **Supp. Figure 2E**. After acute LRRK2 inhibition or in mutants that are dephosphorylated at Ser910/935 (e.g. R1441C/G/H and Y1699C) LRRK2 forms skein or punctate structures in the cytoplasm of cells. Staining for endogenous p62 revealed an increase in co-localization with LRRK2 skeins and puncta over time. Using CRISPR/Cas9, we generated an H1299 cell line targeted with

GFP at the endogenous start-codon of LRRK2 to confirm interaction of LRRK2 and p62 with an alternate tag and cell background, described in **Supplemental Figure 1**. We found that endogenous GFP-LRRK2 interacts with p62. Together, these data show that LRRK2 and p62 interact and confirm previously reported data from Park et al, showing endogenous interaction (62).

Identification of the p62 and LRRK2 Interaction Domains

LRRK2 and p62 are multi-domain proteins with several protein interaction regions. In order to provide insight on downstream biology of the interaction, we determined the interaction domain of p62 on LRRK2 and the interaction domain of LRRK2 on p62 using deletion plasmid constructs. To identify the LRRK2 interaction domain with p62, we expressed GFP-tagged LRRK2 fragments (**Figure 2A**) and analyzed GFP immunoprecipitates for endogenous p62, **Figure 2B**; GFP-tagged LRRK2 is still competent to bind p62 **(Figure 1D)**. The amino terminal armadillo and ankyrin repeat domains of LRRK2 are required for interaction with p62. Fragments of p62 (**Figure 2C**) were expressed in cells expressing GFP-LRRK2 or GFP, and we asked which FLAG-tagged p62 fragments co-precipitated with LRRK2 in GFP immunoprecipitates. We found that the PB1 domain fragment aa1-125 did not interact with LRRK2 when expressed alone, however fragments of p62 that included aa125-225 did interact with LRRK2. We also found that $p62^{118\text{-}440}$ but not $p62^{167\text{-}440}$ precipitated with LRRK2, indicating the ZZ domain [aa118-167] is necessary for interaction with LRRK2 **Figure 2D**. We next sought to determine if this is a direct interaction using recombinant p62 and LRRK2. FLAG-tagged $p62^{118\text{-}225}$ was unstable when expressed in cells, precluding conclusions about interaction using this approach. We did however ask if full-length recombinant FLAG-tagged LRRK2 could be isolated with bacterially expressed full-length p62 or the minimal p62 binding domain identified in **Figure 2D** [$p62^{118\text{-}225}$]. GST or GST-p62 or GST $p62^{118\text{-}225}$ were incubated with full-length LRRK2 and protein complexes were retrieved with glutathione sepharose and analyzed by immunoblot. We found that LRRK2 was co-precipitated with GST-p62 and GST-$p62^{118\text{-}225}$, but not GST alone, **Figure 2E**.

LRRK2 phosphorylates p62 on Thr138.

p62 is regulated by phosphorylation by Casein kinase 2, TBK1/IKKε, p38δ and ULK1 to regulate its cellular functions. We therefore asked if LRRK2 not only bound p62, but could also phosphorylate it as well. Using recombinant p62 and recombinant LRRK2, our initial analysis indicated that LRRK2 could indeed phosphorylate p62. In order to analyze p62 phosphorylation by LRRK2 and determine the phosphorylation site (s), recombinant p62 was expressed as a GST fusion protein and following purification on glutathione sepharose, the GST tag was removed by cleavage with precision protease. Full length recombinant LRRK2, purified from mammalian cells as an amino-terminal FLAG tagged protein, was used to phosphorylate p62 (**Figure 3A)**. Detailed OrbiTrap mass spectrometry analysis of *in vitro* kinase reaction products revealed several potential sites of phosphorylation. The table in **Figure 3** shows the sites of phosphorylation cumulatively identified over several MS determinations (shown in **Supp. Figure 3**) with A score and localization probabilities indicated and spectral counts for the number of times the peptide has been observed (Spc). Because LRRK2 binds p62 through its ZZ domain, we further investigated the sites identified within this domain and generated p62 phosphosite mutant T138A, T164A, S176A recombinant proteins. p62 T138A, T164A, T138A/T164A, S176A and T138A/T164A/S176A were subjected to *in vitro* kinase reactions with $LRRK2^{970\text{-}2527}$ [G2019S] recombinant protein. We found decreased LRRK2-mediated phosphorylation when Thr138 was substituted with Ala, while T164A and S176A had no impact (**Supp. Figure 4**), indicating that the Thr residue at position 138 is the likely site of LRRK2 modification.

Validation of LRRK2 phosphorylation of p62 Thr138

We generated a phosphospecific antibody against phosphothreonine 138 (pThr138) to validate the mass spectrometry phosphosite analyses and track p62 modification. This antibody is specific for the phosphoThr138 peptide, and does not detect dephospho-peptide as shown in **Supp. Figure 4B.** To test this antibody on p62, we compared p62 to p62 T138A phosphorylation by LRRK2$^{970\text{-}2527}$ [G2019S] recombinant protein in the presence or absence of LRRK2 inhibitor GNE1023 (**Figure 3B**, left panel) and full length LRRK2$^{1\text{-}2527}$ and kinase inactive LRRK2$^{1\text{-}2527}$ [D1994A] (**Figure 3B**, right panel). Similar to **Supp. Figure 4**, we found that LRRK2 preferentially phosphorylates Thr138. Our antibody specifically recognizes p62 phosphorylated at Thr138 by LRRK2 on wild-type p62 but neither on p62 T138A nor in reactions where inactive LRRK2 or LRRK2 inhibitor was included. We tracked LRRK2 kinase activity with a pThr1491 antibody, which reveals LRRK2 autophosphorylation kinase activity was absent in the presence of the kinase inactive mutant D1994A.

LRRK2 Phosphorylates p62 in cells

Thus far, we have found that LRRK2 forms an endogenous complex with p62 in cells and that LRRK2 can phosphorylate p62 *in vitro*. We next sought to determine if LRRK2 could phosphorylate p62 in cells and if inhibition of LRRK2 would suppress p62 phosphorylation at Thr138. We examined the dose effects of MLi-2 inhibition of LRRK2 in cells expressing GFP-LRRK2 [WT, D2017A, and G2019S] and FLAG-p62 [WT and T138A]. We found that, similar to the bone fide Rab GTPase substrates, concentrations of 3-30nM MLi-2 decreased p62 phosphorylation at T138A, **Figure 4A**. We tracked the effects of the potent LRRK2 inhibitor with pSer935 and pSer1292 antibodies; dephosphorylation of the autophosphorylation site (Ser1292) and the upstream kinase site (Ser935) were concomitant with p62 dephosphorylation. We observed a similar reduction in p62 phosphorylation using two other structurally diverse inhibitors, PF745 and GNE1023, with IC50 values below 100nM, compared to an IC50 of below 10nM for MLi-2 (**Supp. Figure 5 A and B**). We used MLi-2 on control EBV-transformed lymphoblasts to ask if inhibition of endogenous LRRK2 activity blocks endogenous p62 phosphorylation at pThr138. We found that 10nM MLi-2 reduces the phospho Thr138 signal on p62 immunoprecipitates (**Figure 4B**), demonstrating p62 is an endogenous substrate of LRRK2. We next compared the rate of dephosphorylation of LRRK2 and p62 pThr138 after inhibition with MLi-2. We found that LRRK2 autophosphorylation is reduced within 10 minutes, while pSer935 and pThr138 is ablated by 40 minutes (**Figure 4C**). To verify LRRK2 inhibitor treatment was specific to blocking LRRK2 activity, we employed the A2016T mutation of LRRK2 which shows reduced sensitivity to LRRK2 inhibitors. Treatment of cells expressing p62 and wild-type LRRK2 with MLi-2 showed reduced p62 phosphorylation but not treatment of cells expressing A2016T with p62, **Figure 4D**.

The dephosphorylation of p62 Thr138 is rapid, revealing a phosphatase activity against this site. In order to determine if PP1 or PP2 type phosphatases are responsible for p62 dephosphorylation, we employed a pharmacological approach using Okadaic acid to inhibit PP2 and Calyculin A to inhibit PP1. Previously, we showed that Calyculin A prevents LRRK2 inhibitor induced dephosphorylation (81). **Figure 5** shows that inclusion of 100nM Okadaic acid does not affect p62 dephosphorylation in the presence of 10nM MLi-2, while 20nM Calyculin A enhances p62 phosphorylation on its own, and also prevents dephosphorylation when co-treated with 10nM MLi-2 for 30 minutes, implicating PP1-type and not PP2-type phosphatases in the dephosphorylation of LRRK2 phosphorylated p62.

A Subset of Pathogenic PD-Associated LRRK2 Mutations Enhance p62 Phosphorylation

Pathogenic PD mutations found in the Roc/COR and kinase domains exhibit increased kinase activity in cells, as measured by autophosphorylation of pSer1292 and phosphorylation of downstream Rab GTPase substrates. Since we found that LRRK2 phosphorylates p62 in cells

and discovered p62 to be a bone fide substrate of LRRK2, we next investigated if pathogenic PD mutations modulate p62 phosphorylation similar to what has been reported for LRRK2 kinase activity in vitro and against Rabs in cells. To do this, we expressed GFP-LRRK2 [WT, N1437H, R1441G, Y1699C, G2385R, and G2019S] and FLAG-p62 WT in cells and analyzed p62 phosphorylation, **Figure 6A**. Immunoblotting with anti-pThr138 antibody, we found Thr138 phosphorylation was only observed with active LRRK2 mutants and dramatically reduced in GFP vector control or kinase inactive LRRK2 (D2017A). LRRK2 N1437H, R1441G, Y1699C and G2019S display increased p62 Thr138 phosphorylation, compared to wild-type kinase, **Figure 6A** and quantitated in **Figure 6B**. We observed increased kinase activity in N1437H, R1441G, Y1699C and G2019S LRRK2 in cells with the pSer1292 antibody, similar to the increase in p62 phosphorylation. We observed decreased kinase activity of I2020T and G2385R LRRK2 by pSer1292 and p62 pThr138 immunoblotting, which reflects previous analyses of these LRRK2 mutants (90,91). In line with similar reports, LRRK2 pSer935 is decreased in N1437H, R1441G, Y1699C, and G2385R.

There are discrepancies between the observed increased kinase activity of Roc/COR mutants (e.g. R1441C/G, Y1699C) *in vivo* and lack thereof *in vitro.* Increased pSer1292 and Rab phosphorylation is observed in cells, where only slight increases in activity on peptide substrates (Nictide and LRRKtide) or native protein substrates (Rabs) are found *in vitro (58,90,91)*. We therefore asked if the phosphorylation pattern of p62 was similar *in vitro* with the same LRRK2 mutants. We used full-length recombinant LRRK2 proteins harboring the R1441G, Y1699C, G2019S, and G2385R mutations and compared phosphorylation of recombinant, tag-free p62 protein and recombinant tag-free Rab8 for *in vitro* kinase assays. As was observed previously for the Rab substrates (58), we observed increased phosphorylation with LRRK2 G2019S and diminished phosphorylation with the G2385R mutation, while we observed similar phosphorylation of p62 by R1441G and Y1699C compared to wild-type protein, **Figure 6C**. Given that these mutations show similar activity as wild-type protein *in vitro,* but increased activity in cells, these results indicate that the increased activity of the Roc/COR mutations observed in cells could be mediated by a cellular factor or event as proposed in (58).

LRRK2 Amino Terminus is required for optimal substrate phosphorylation

We mapped the interaction domain of LRRK2 and p62 to the amino terminus of LRRK2 and the ZZ domain of p62. We therefore examined whether structural deletions of the LRRK2 interaction domain with p62 would impact regulation of p62. We tested LRRK2$^{\mathbf{1\text{-}2527}}$, LRRK2$^{\mathbf{970\text{-}2527}}$, and LRRK2$^{\mathbf{1326\text{-}2527}}$, all shown to be active in their recombinant form, for their ability to phosphorylate p62 in cells. We found that deletion of the LRRK2 amino terminus ablates p62 phosphorylation by LRRK2$^{\mathbf{970\text{-}2527}}$ and LRRK2$^{\mathbf{1326\text{-}2527}}$ proteins, **Figure 7A**. We next asked if the amino terminus is similarly needed to regulate Rab substrates Rab7L1, Rab8 and Rab10. LRRK2 phosphorylation of Rab7L1 tracked similar to p62, where both LRRK2$^{\mathbf{970\text{-}2527}}$ and LRRK2$^{\mathbf{1326\text{-}2527}}$ did not phosphorylate Rab7L1 at Thr71, **Figure 7B** left panel. Interestingly, LRRK2$^{\mathbf{970\text{-}2527}}$ was able to phosphorylate both Rab8 and Rab10, though LRRK2$^{\mathbf{1326\text{-}2527}}$ was unable to modify these Rabs, **Figure 7B** middle and right panels. These data further implicate the amino terminus of LRRK2 in regulation of its kinase activity against certain substrates. Ito et al. showed that blocking LRRK2 phosphorylation at Ser935 significantly reduced Rab10 phosphorylation (92); we therefore determined whether regulation of the crucial phosphorylation sites Ser910/935 is involved in p62 regulation. To investigate this, we expressed p62 in cells expressing WT, D2017A, and S910/935A LRRK2, and found that although S910/935A is active [pSer1292], it does not phosphorylate p62, **Figure 7C**.

The Carboxy Terminus of p62 Influences its Phosphorylation by LRRK2

A previous report indicates that there is interplay in the regulation of pSer407 and pSer403 in p62. We therefore wanted to understand if there could be any impact of the carboxy terminus or

its phospho-regulatory sites on the phosphorylation of p62 by LRRK2. This was accomplished by mutating these sites to alanine or phosphomimetic glutamate and asking if this would alter LRRK2 phosphorylation of Thr138. We saw that neither S403A or S407A alanine substitutions nor the phospho-mimetic glutamate substitutions, S403E (which also cross-reacts with anti-pSer403 antibodies) or S407E significantly altered LRRK2 G2019S phosphorylation on Thr138, **Figure 8A**. However, removing the ability of p62 to bind ubiquitin blocked Thr138 phosphorylation. Phe406 in the UBA domain of p62 is crucial for ubiquitin binding and we found that substitution of Phe406 with Valine, a mutation known to reduce ubiquitin binding to p62 (25,93), decreased the LRRK2 phosphorylation of p62 Thr138, **Figure 8A.** Similarly, when we deleted the UBA domain we also reduced p62 phosphorylation at Thr138, **Figure 8B**, despite maintaining its interaction with LRRK2, **Figure 2**.

p62 Contributes to LRRK2-mediated Neuronal Cell Death

Expression of PD associated mutants of LRRK2 in primary neuronal cultures induces cell toxicity including neurite shortening and apoptosis (60,94-98). To determine if p62 contributes to mutant LRRK2 induced neuronal cell toxicity, we expressed wild-type LRRK2 or mutant LRRK2 [G2019S] with p62 or p62 T138A, **Supplemental Figure 6** and **Figure 9**. We observed intense colocalization of LRRK2 with p62 and condensed nuclei, **Figure 9A.** The classical apoptotic nuclear morphology co-localized with activated caspase-3 immunostaining, **Figure 9A** (red). When these cells were scored for the percentage of transfected neurons exhibiting condensed nuclear morphology, we found that G2019S increases the percentage of cells with condensed nuclei that stain positive for caspase 3, over wild-type LRRK2 or p62 expression alone. However, the LRRK2 unphosphorylatable mutant p62 Thr138Ala fails to enhance the toxicity of mutant LRRK2, **Figure 9B**. Representative image of neuronal culture purity as indicated by βIII-Tubulin staining is shown in **Figure 9C**. Additional representative images of neurons expressing p62 (and LRRK2), and labeled for active caspase-3 are shown in **Supplemental Figure 7**. Here we show that co-expression of LRRK2 [G2019S] with p62 significantly increases the number of apoptotic neurons.

Discussion

Almost 15 years after the LRRK2 locus was found to be associated with Parkinson's disease, only a subset of endogenous substrates have been highly validated in the field (51,58,99), namely the Rab GTPases. In the present study, we contribute another protein to this repertoire of LRRK2 substrates, the signaling adapter p62/SQSTM1. We showed that p62 is an endogenous interactor of LRRK2. Using mass spectrometry and mutational analysis, we found that LRRK2 phosphorylates p62 on Thr138 *in vitro*. Using a specific pThr138 antibody that readily detects p62 phosphorylated on Thr138, we then showed that p62 phosphorylation is diminished in cells treated with specific and selective LRRK2 inhibitors and that PD associated mutations in LRRK2 (N1437H, R1441G, Y1699C and G2019S) increase p62 phosphorylation. The precise mechanism of how p62 Thr138 phosphorylation alters its downstream function in established pathways is still to be investigated. However, we report here that when p62 and mutant LRRK2 are introduced together in primary neurons, a synergistic lethality is observed with increased apoptosis (**Figure 9**), which is rescued by mutation of Thr138 to Ala.

We originally observed p62 association with LRRK2 in a targeted screen of multiple putative interacting chaperone and adapter proteins. Hsp27 provides thermotolerance and stabilization of denatured protein for remedy by refolding chaperones (100,101), and interacts with LRRK2. We and others have previously identified Hsp90 and Cdc37 interacting with LRRK2 (86,87,102-105). Hsp70 and Hsc70 are also known LRRK2 interacting proteins (64). Expression of Hsp110, a protein disaggregase alone did not interact with LRRK2. HDAC6 and p62 facilitate the removal of aggregated and ubiquitinated proteins and interestingly, these

proteins specifically co-immunoprecipitated with LRRK2. LRRK2 was recently reported to interact with acetylated microtubules, which are produced by enhanced HDAC6 activity (106), supporting LRRK2 as playing a regulatory role for HDAC6. Endogenous LRRK2 interacts with endogenous p62, and the specificity of this interaction is demonstrated by the more selective co-immunoprecipitation with LRRK2 instead of LRRK1**, Figure 1**. LRRK1 domain structure is very similar between LRRK2 and LRRK1, except for divergent amino termini. This likely explains the identification of the LRRK2 amino terminus as the interaction domain with p62 [**Figure 2**]. We additionally found that p62 binds to the LRRK2 armadillo domain through its ZZ domain [$p62^{118-225}$], which is similar to what was seen in Park et al. 2016 (62). There is overlap in the conclusion but a slight discrepancy in the results, which could be due to the use of internal deletion constructs (62) versus expression tagged fragments used here. Typically, we observe an enhanced interaction of LRRK2 and p62 in the presence of LRRK2 inhibitors, however this may be context dependent or transient.

Some kinases interact with their substrates stably (107) and this is true for LRRK2 and p62. We mapped Thr138 on p62 as a specific site of LRRK2 phosphorylation, and we developed phospho-specific antibodies against this site. Interestingly, a tryptic peptide from p62 that encompasses the Thr138 site has been identified in multiple studies (108-111) but with di-Gly linkage on the Lys at the +3 position from Thr138; this could have precluded or complicated identification of pThr138 in unbiased phospho-proteomic screens and increased our technical difficulty in detecting endogenous pThr138. We established a dependence of LRRK2 activity for phosphorylation of p62 Thr138 in cells using three structurally distinct inhibitors. Using the specific inhibitor MLi-2, LRRK2 phosphorylation of p62 was blocked within 40 minutes, and was restored with the inhibitor resistant mutant [A2016T]. Importantly, we found that inhibition of endogenous LRRK2 decreased p62 phosphorylation on Thr138 in lymphoblasts (**Figure 4B**). Having established that blocking LRRK2 kinase activity results in decreased p62 phosphorylation, we next characterized the in vivo phosphatase activity on p62. The downstream target p62 was dephosphorylated at a similar IC_{50}, but at a more rapid rate than pSer1292 (**Figure 4**). The rapid dephosphorylation of p62 indicates that a phosphatase actively regulates p62. The LRRK2 signaling pathway has been implicated to involve PP1 and possibly PP2A, (112) in the role of Ser935 dephosphorylation. Using a pharmacological approach, we narrowed the class of phosphatases involved in p62 Thr138 dephosphorylation to PP1-type enzymes, and possibly PP2A (**Figure 5**).

We found that pathogenic PD-associated LRRK2 mutants [N1437H, R1441G, Y1699C and G2019S] enhance the phosphorylation of p62 in cells. However, this enhancement was only observed with G2019S *in vitro*, compared to the R1441G and Y1699C mutants. This reflects similar modification patterns observed with the recently reported Rab substrates comparing in vitro to in vivo activity of LRRK2 (58). This could be due to cellular factors or localization differences in cells that are not present *in vitro*, that contribute to the regulation of LRRK2 kinase activity. The risk factor mutation G2385R, which was reported to have decreased activity and reduced Ser935 phosphorylation (103), exhibited reduced phosphorylation of p62 in cells and *in vitro*, similar to the Rab substrates, **Figure 6**. We observed that the I2020T mutation did not increase LRRK2 phosphorylation of p62, raising important distinctions in biochemical changes caused by different disease or risk enhancing mutations. These data indicate that, similar to pSer935 and phospho-Rab substrates, p62 pThr138 is a viable pharmacodynamic marker and activity marker for LRRK2.

There is yet to be a crystal structure of full-length LRRK2; however, a molecular model, derived from cryo-EM and cross-linking studies, provides useful insight into the general organization of the dimer (113), with other structural studies in general support (114,115). The amino terminus appears to lay across the Roc-COR domain interface to regulate activity. In support of this, Ito et al determined that phosphorylation of LRRK2 pSer910/935 is necessary for Rab 10 phosphorylation(92). In the context of the novel substrate p62, we found that

pSer910/935 is also necessary for p62 Thr138 phosphorylation. Using LRRK2 amino terminal deletion mutants, we showed that the amino terminus influences phosphorylation of p62 and Rab substrates. It is therefore likely that phosphoregulation of the LRRK2 amino terminus (e.g. Ser910/935/955/973) indirectly regulates LRRK2 substrate phosphorylation and therefore the kinases and phosphatases that modify LRRK2 are prime targets for elucidation. This is distinct from *in vitro* conditions (**Figure 3**), where LRRK2$^{970\text{-}2527}$ is able to phosphorylate p62, but it is however further reflective of the differences in LRRK2 kinase activity observed *in vitro* versus in cells as is seen with Roc/COR mutants. This is also the case for the Rab proteins, where LRRK2$^{970\text{-}2527}$ is able to phosphorylate Rabs in vitro (58), but pSer910/pSer935 are required in cells (92).

There are consistent reports of LRRK2 modulation of the autophagic process. However, the mechanistic role of LRRK2 in regulating autophagy has been elusive to date, i.e. no members of the autophagic machinery (i.e. ATG proteins) have been shown to be validated LRRK2 kinase substrates. p62 is phosphorylated by multiple kinases throughout several domains to regulate its function and many of these phosphorylation events have been shown to have interdependent regulation. We show that the carboxy terminal ubiquitin binding domain of p62 influences the phosphorylation of the ZZ domain by LRRK2. It is therefore possible that the ubiquitin binding function of p62, a crucial aspect of its autophagic role, feeds into LRRK2 regulation of p62 and thus autophagy. Therefore, the ubiquitin binding function of p62 bridges LRRK2 activity to autophagy regulation, where the impact of hyperphosphorylation of p62 will need to be investigated.

Our data linking p62 to LRRK2 Parkinson's disease supports previous reports of p62 involvement with aggregated αSyn protein inclusions in PD as well as in other neurodegenerative diseases, including amyotrophic lateral sclerosis (ALS), polyglutamate disorders, and multiple system atrophy (MSA) (3-11). p62 binds to synuclein inclusions and pathology increases in the contralateral hemisphere from fibrillar αSyn injection (116). This places p62 intracellularly with endogenous αSyn and also inclusions in cells affected by synuclein through uptake from the extracellular milieu. Interestingly, cytoplasmic aggregates of LRRK2 expressed in cell culture and primary neurons colocalize with p62 (44). Furthermore, p62 knockout in a αSyn transgenic mouse has been found to increase Lewy body like pathology (117).

p62 is involved in multiple cellular processes that could indeed intersect with reported functions of LRRK2, from mitochondrial maintenance to vesicular trafficking (12,13,15,18,46,62,63,65,118-125). For LRRK2, expression of PD associated mutants in cultured neurons leads to enhanced cell toxicity (61,94,95). When we asked if p62 modulated this phenotype we indeed found a synergistic toxic effect of mutant LRRK2 and p62 expression, dependent on Thr138 (**Figure 9**). It is possible that in this context, over-expressed hyperphosphorylated p62, co-expressed with G2019S-LRRK2, fails to activate the Nrf2 cytoprotective pathway similar to that recently reported in cultured neurons in which elevated levels of phosphorylated p62 (at Ser351) are observed following proteasome inhibition (126). In fact, it was recently shown that upregulating Nrf activity decreased LRRK2 neuronal toxicity (79). We have identified a cooperative role of p62 in LRRK2 kinase activity dependent toxicity, but delineating the effects on other p62 functions are the topics of future studies. The interplay of p62 phosphorylation on disease pathogenesis is only now being uncovered and indeed, there are other LRRK2 influenced phosphorylation sites (62), further linking the phosphoregulation of p62 to PD. In conclusion, this work identifies p62 as a novel substrate of LRRK2. With this novel substrate we validate the necessity of the amino terminus for LRRK2 substrate phosphorylation and uncover p62 as a potential mediator of PD-mutant LRRK2 toxicity.

Acknowledgements

The Authors would like to thank the Brin/Wojcicki Foundation and the Michael J. Fox Foundation for funding this work. We would also like to thank Troomonos Mou for technological assistance. We are grateful to Dario Alessi for providing MLi-2, Rab antibodies and plasmid reagents. We are also grateful to the many plasmid depositors from Addgene.

Conflict of interest-The Authors declare no conflicts of interest.

Author Contributions-RJN conceived and designed the study, JZ originally observed the LRRK2-p62 interaction. AFK, JZ, MFB, AM, SN, TPM, WHW and HJR and RJN conducted and analyzed the experiments. AFK, HJR and RJN wrote the manuscript.

Figure Legends

Figure1. LRRK2 interacts with p62/SQSTM1.

(**A**) Plasmids encoding V5-tagged Hsp27, DNAJB6 (Hsp40), DNAJB8 (Hsp40), HSPA1A (Hsp70), HspA8 (Hsc70), Hsp90, HSPH1 (Hsp110) and FLAG-tagged HDAC6 and FLAG-p62 were transfected into GFP or GFP-LRRK2 wild-type T-REx HEK293 cells. GFP immunoprecipitates from 1% NP40 soluble cell lysates were subjected to immunoblot with α-GFP, α-V5 (chaperones) and α-FLAG (HDAC6 and p62). (**B**) HA-p62 was co-expressed with FLAG vector, FLAG-LRRK2 or FLAG-LRRK1 in HEK293 cells. 48hrs post-transfection, cells were treated with GNE1023 for 90min and α-FLAG immunoprecipitates were blotted with α-HA (p62), α-FLAG (LRRK2/LRRK1) α-Hsp90 and α-LRRK2 pSer935 and pSer1292. *Lower panel* LiCOR quantitation of the α-HA/α-FLAG signals set to LRRK2, no inhibitor control; n=3 one sample *t*-test set to the hypothetical value of 1, $*p \leq 0.05$ (**C**) A549 cells treated ± 2μM GNE1023 were subjected to LRRK2 immunoprecipitation with α-LRRK2 (UDD3) and immunoprecipitates were subjected to immunoblot with α-LRRK2 (N241, pSer1292 and pSer935) and α-p62. (**D**) Endogenous GFP-LRRK2 H1299 cell lines generated by CRISPR/Cas9 editing were subjected to GFP-Trap immunoprecipitation; Lysates and immunoprecipitates were blotted for the presence of LRRK2, p62, Hsp90 and 14-3-3 proteins. *Generation of CRISPR/Cas9 lines described in Supplemental material.*

Fig 2. Interaction Domains of p62/SQSTM1 and LRRK2.

Structures and the deletion constructs of LRRK2 (**A**) and p62/SQSTM1 (**C**) are shown. **B.** LRRK2 interaction domains with p62/SQSTM1. HEK293 cells were transfected with indicated GFP tagged LRRK2 constructs. GFP-TRAP immunoprecipitates were immunoblotted for endogenous p62 (α-p62), and Hsp90. Binding of endogenous p62/SQSTM1 is represented qualitatively in **A** with – or +. (**D**) GFP or GFP-LRRK2 WT T-REx cells were transfected with indicated FLAG tagged p62/SQSTM1 fragment constructs. 48hrs after transfection, cells were harvested and subject to GFP-IP as described. GFP antibody showed the loading quantity of GFP-LRRK2. FLAG antibody indicated the amount of expressed FLAG-p62/SQSTM1 pulled down by GFP-LRRK2. The binding ability of expressed p62/SQSTM1 fragments were presented with – or + in **C.** (**E**) LRRK2 and p62/SQSTM1 interacts in cell free context. In *in vitro* binding assay, bacterially expressed GST, GST-p62/SQSTM1 full length or GST-p62/SQSTM1$^{118\text{-}225}$ were incubated with full length FLAG-LRRK2 G2019S. The protein complexes were retrieved with glutathione sepharose and immunoblotted for LRRK2 (N241). GST blots indicate GST, GST p62/SQSTM1 full length or fragment bait retrieved.

Figure 3. Identification of residues on p62 phosphorylated by LRRK2.

(**A**) E. coli expressed p62$^{1\text{-}440}$ (2.5μM) was reacted with 200nM full length LRRK2$^{1\text{-}2527}$ [G2019S] *in vitro* with cold ATP. The colloidal blue stained band corresponding to p62 was excised and analyzed by Orbitrap mass spectrometry. The table presents the total number of peptide spectral counts identified from 10 individual reactions, along with the best A score and localization probability (129) for each site. Extended results from individual reactions and MS analyses are in Supplemental Figure 2. (**B**) Left panel, 3 μM recombinant wild type p62 or T138A were reacted with 93nM LRRK2$^{970\text{-}2527}$ in the absence or presence of 1μM GNE1023 with [γ-32P]-ATP. Right panel, 3 μM recombinant wild type p62 or p62 [T138A] were reacted with 56nM full length LRRK2$^{1\text{-}2527}$ G2019S or kinase inactive LRRK2$^{1\text{-}2527}$ [D1994A]. Reaction products were analyzed by coomassie blue staining, autoradiography and immunoblot using anti-p62 pThr138 immunoblot (αpThr138). LRRK2 kinase activity was tracked with (αpThr1491) antibodies and αLRRK2 (N241).

Figure 4. LRRK2 phosphorylates p62 Thr138 in cells.
(**A**). GFP, GFP-LRRK2 wildtype, kinase inactive [D2017A] or G2019S were expressed along with FLAG-p62 or FLAG-p62 T138A in HEK293. Cells were treated with the indicated concentrations of MLi-2 (0-30nM) for 90 minutes. Equal amounts of anti-FLAG immunoprecipitates were analyzed by pThr138 and p62 immunoblot. Cell lysates were probed for LRRK2 (αGFP and N241), phospho-LRRK2 (αpSer1292 and αpSer935) and actin. (**B**) Human EBV-transformed Lymphoblasts were grown in suspension and treated with 10nM MLi-2 (90min). Endogenous p62 immunoprecipitates from monoclonal αp62 (MBL) IPs were analyzed by αpThr138, αpSer403 and total αp62. Lysates were probed for total and phosphorylated LRRK2 (αN241/αpSer935), p62 and actin. (**C**) Wild-type GFP-LRRK2 was expressed with FLAG-p62 and treated for the indicated times with 10nM MLi-2 and analyzed as in (**A**). (**D**) T-REx lines harboring the indicated LRRK2 variants (GFP-LRRK2 WT, kinase inactive [D2017A] or LRRK2 [A2016T]) were transfected with FLAG-tagged p62 WT or p62 T138A and induced with 1μg/mL doxycycline for 48 hours and treated ± 10nM MLi-2 for 90min prior to harvest. p62 immunoprecipitates were analyzed for pThr138 as in **A** and **C**.

Figure 5. p62 pThr138 is regulated by a Calyculin A sensitive phosphatase.
Cells co-expressing GFP, GFP-LRRK2, or GFP-LRRK2 G2019S and wild-type FLAG-p62 were treated with 10nm MLi-2, 100nm Okadaic acid alone or simultaneously with 10nm MLi-2 for 30 min (left panel). In the right panel, cells co-expressing GFP, GFP-LRRK2, or GFP-LRRK2 G2019S and wild-type FLAG-p62 were treated with 10nm MLi-2, 20nm Calyculin A alone or simultaneously with 10nm MLi-2 for 30 min. Anti-FLAG immunoprecipitates were analyzed for changes in p62 phosphorylation by αpThr138 immunoblot. LRRK2 phosphorylation responded as was previously reported with the antibodies for total LRRK2 (αGFP and N241) and phospho-LRRK2 (αpSer1292 and αpSer935).

Figure 6. Effects of pathogenic PD-associated LRRK2 mutations on p62 phosphorylation in cells and in vitro.
(**A**) Plasmids encoding GFP, GFP-LRRK2 [N1437H, R1441G, Y1699C, G2019S, I2020T and G2385R] PD mutations were transfected along with FLAG-p62 wild-type in HEK293 cells. Anti-FLAG immunoprecipitates were analyzed for changes in p62 phosphorylation by αpThr138 immunoblot. LRRK2 phosphorylation was assessed by immunoblot with total LRRK2 (αGFP and N241) and phospho-LRRK2 (αpSer1292 and αpSer935). (**B**) Quantification of the phosphorylation change is expressed as the ratio of phosphorylated p62 at Thr138 over total p62 signal as analyzed via LiCor Odyssey and normalized to wild-type LRRK2. n=3, means±s.e.m. (**C**) 35nM full- length recombinant LRRK2 [WT, D1994A, R1441G, Y1699C, G2019S, and G2385R] was reacted with 3μM p62 or Rab8 and with [γ-32P]-ATP. Reaction products were analyzed by coomassie blue staining, autoradiography and immunoblot with anti-p62 pThr138 immunoblot (αpThr138), rabbit total p62 (MBL), sheep anti-phospho Rab8 and total Rab8 (CST). LRRK2 kinase activity was tracked with αpThr1491 and total LRRK2 was detected with αLRRK2 (N241).

Figure 7. The LRRK2 amino terminus and Ser910/935 phosphorylation are required for optimal substrate phosphorylation. (**A**) Full length GFP-LRRK2 WT and D2017A (KD), GFP-LRRK2$^{970\text{-}2527}$ and GFP-LRRK2$^{1326\text{-}2527}$ were co-expressed with FLAG-p62 wild-type or FLAG-p62 T138A, in the presence or absence of 10nM MLi-2. FLAG immunoprecipitates were probed for p62 pThr138 and lysates were blotted for LRRK2 (N241) and phospho-LRRK2 αpSer1292 and αpSer935 (**B**) Full length GFP-LRRK2 WT and D2017A (KD), GFP-LRRK2$^{970\text{-}2527}$ and GFP-LRRK2$^{1326\text{-}2527}$ were co-expressed with Rab7L1 (left panel), Rab8A (middle panel) or Rab10 (right panel) and their indicated variants. Cell lysates were probed for phospho-Rab7L1 Thr71,

phospho-Rab8 Thr72, and phospho-Rab10 Thr73, or total LRRK2 (N241) and phospho-LRRK2 (αpSer1292 and αpSer935). (**C**) FLAG-tagged p62 WT was expressed in T-REx HEK293 cells stably expressing GFP, GFP-LRRK2 WT, GFP-LRRK2 D2017A, and GFP-LRRK2 [S910/935A] and cells were simultaneously induced to express LRRK2 by inclusion of 1μg/mL doxycycline in the culture media. Cells were treated ±10nm M-Li2 for 90 minutes prior to harvest. FLAG immunoprecipitates were probed for p62 pThr138 and lysates were blotted for LRRK2 (N241) and phospho-LRRK2 αpSer1292 and αpSer935.

Figure 8. The p62 UBA domain is necessary for LRRK2 phosphorylation at Thr138. (**A**) The indicated p62 mutants were transiently expressed in HEK293 cells along with either GFP-LRRK2 WT, FLAG-IKKε, GFP-LRRK2 kinase dead (KD) [D2017A], or GFP-LRRK2 G2019S. FLAG immunoprecipitates were probed for p62 pThr138 and pSer403. Lysates were blotted for LRRK2 (N241), phospho-LRRK2 αpSer1292 and αpSer935, and actin. (**B**) FLAG-p62 WT, FLAG-p62 F406V, or FLAG-p62 [aa1-380] were co-expressed with GFP-LRRK2 WT and GFP-LRRK2 G2019S in HEK293 cells and analyzed as in **A**.

Figure 9. p62 participates in mutant LRRK2-induced neuronal death signaling. (**A**) Primary rat embryonic cortical neurons, prepared as in **Supplemental Figure 5**, were co-immunostained for anti-Flag (green) and anti-active caspase-3 (red), together with DAPI (blue). (**B**) The stained coverslips were observed under 40X magnification, and neurons double positive for EGFP and FLAG were scored according to their nuclear morphology. Neurons were considered to be apoptotic if two or more condensed chromatin bodies were observed within a neuronal profile. 100 positive neurons in each experiment were counted by a blinded rater, and apoptotic neurons were expressed as a percentage of neurons positive for both FLAG and EGFP. mean ±s.e.m. N=3, one-way ANOVA with Tukey's post-hoc test; P*<0.05, P***<0.001. (**C**) Parallel coverslips of primary rat cortical neurons were co-transfected with LRRK2 (pcms-EGFP) and Flag-p62, and the fixed cultures stained for mouse anti-βIII-Tubulin (Tuj-1; red) and rabbit anti-Flag (magenta), with DAPI (blue). Images were obtained on a Leica TSP5 confocal microscope.

Supplemental Figure 1. (A) General scheme of locus and repair template. (**B**) Genomic DNA from 4 targeted clones and two scrambled clones were amplified with the primers surrounding the cleavage site PCR products were analyzed by gel electrophoresis. Variable lengths of targeted loci are found compared to no insertions from the scrambled gRNA control lines.

Supplemental Figure 2. Detection of LRRK2:p62 complexes by PLA. (**A**) FLAG vector, FLAG-HDAC4 or FLAG-p62/SQSTM1 were transfected into T-REx WT GFP-LRRK2 cells. *In situ* Proximity Ligation Assay (PLA) assay was performed using α-GFP (LRRK2) and α-FLAG (p62 or HDAC4). The top panel shows PLA signals in GFP-LRRK2/FLAG-p62 expressing cells with single antibody GFP or FLAG controls. The bottom left-hand panels show the merged image of cells stained with DAPI (blue) and ligation amplifications (red). A merged image of GFP-LRRK2 with DAPI/PLA is presented in the middle column. PLA signals per cell were quantitated by Duolink ImageTool and are presented as fold change from the number of vector signals per cell from *n*=3 experiments. Results are means± s.e.m., analysis was one-way ANOVA against each control (*$P < 0.05$). The right-hand panels show immunocytochemistry (ICC) with anti-FLAG antibody staining of transfected HDAC4 or p62. The merged image shows DNA (blue), GFP–LRRK2 (green) and FLAG–HDAC4 or p62 (red). (**B**) Representative negative control images of T-REx cells subjected to PLA. The top two rows show merged images of PLA signal detection (Red) in GFP-LRRK2 expressing T-REx cells (green) transfected with FLAG-p62/SQSTM1 or FLAG-HDAC4. PLA was carried out with only one primary antibody (indicated). The bottom left image shows signal detection in LRRK2 absent cells with both GFP and FLAG

antibodies. Signals from these controls are included with the quantitation graph of PLA signals/cell from **Figure 1B** in the bottom right. (**C**) A549 cells treated ± 0.1μM MLi2 at different times, for four hours, were subjected to LRRK2 immunoprecipitation with α-LRRK2 (UDD3) and immunoprecipitates were subjected to immunoblot with α-LRRK2 (N241 and pSer935) and mouse α-p62 (MBL). α-p62/α-LRRK2 LiCOR quantitation is shown in the lower panel; t-test, *p≤0.05. (**D**) PLA was performed on A549 cells treated ± 2μM GNE1023 using control rabbit and mouse IgG, α-p62 (MBL) and α-LRRK2 (N241). Results are means± s.e.m., analysis was one-way ANOVA against each control. The representative images of PLA in A549 cells are shown. Images in the top row show single antibody PLA reactions along with IgG control pair antibody. The bottom row includes both anti-LRRK2 (N241) and mouse anti-p62 antibodies. The bottom right panel shows signals from PLA on human lung alveolar epithelial A549 culture treated with 2μM GNE1023 for 1.5hrs. (**E**) A549 cells were transduced with GFP-LRRK2 Bacmam, 24 hrs before GNE1023 (2μM) treatment. Cells were fixed at indicated times following GNE1023 treatment and probed with a SQSTM1/p62 antibody. p62 relocalizes from punctate structures to LRRK2 skeins and inclusions following GNE1023 treatment.

Supplemental Figure 3. In vitro phosphorylation and Mass Spectrometry Mapping of p62 pThr138 phosphorylation by LRRK2. (**A**) Carboxy terminal 6XHis-tagged $p62^{85-440}$ 3μM was reacted with 140nM Full length LRRK2 wild-type, kinase inactive LRRK2 [D1994A], and LRRK2 [G2019S] or $LRRK2^{970-2527}$ [G2019S] in vitro with cold ATP. The colloidal blue stained band corresponding to p62 was excised and analyzed by Orbitrap mass spectrometry. The table presents the total number of peptide spectral counts for each of the reactions, along with the best A score and localization probability (Beausoleil et al. 2006) for each site. (**B**) 140nM $LRRK2^{1-2527}$ [G2019S] was reacted with 2μM GST-tagged $p62^{1-440}$, $p62^{1-380}$, $p62^{118-225}$, or 140nM $LRRK2^{970-2527}$ [G2019S] was reacted with 2μM $p62^{1-440}$ or $p62^{118-225}$. The colloidal blue stained band corresponding to p62 was excised and analyzed by Orbitrap mass spectrometry. (**C**) Reaction and mass spectral counts from **Figure 3A** reaction with 140nM kinase and 2.5μM p62. The colloidal blue stained band corresponding to p62 was excised and analyzed by Orbitrap mass spectrometry. (**D-F**) Representative mass spectra observed from major potential phosphorylation sites identified in the ZZ domain of p62 for pThr138, pThr164 and pSer176.

Supplemental Figure 4. Verification of pThr138 phosphosite by mutagenesis. A. 140nM $LRRK2^{970-2527}$ [G2019S] was reacted with recombinant GST-tagged p62 wild-type, p62 [T138A], p62 [T164A], p62 [T138A/T164A] double mutant, p62 [S176A], and the p62 [T138A/T164A/S176A] triple mutant at 3μM as indicated. Reaction products were resolved by SDS-PAGE and subjected to coomassie blue staining (lower panel) and autoradiography (upper panel). **B.** Phospho-Thr138 and dephosphopeptide were spotted with the indicated amount of peptide and immunoblotted with the anti-phosphoTHr138 antibody.

Supplemental Figure 5. PF475 and GNE1023 inhibit p62 phosphorylation by LRRK2.
(**A**). GFP, GFP-LRRK2 wildtype, kinase inactive [D2017A] or G2019S were expressed along with FLAG-p62 or FLAG-p62 T138A in HEK293 cells. Cells were treated with the indicated concentrations of PF475 (0-3μM) for 90 minutes. Anti-FLAG immunoprecipitates were analyzed by pThr138 and p62 immunoblot. Cell lysates were probed for LRRK2 (αGFP and N241), phospho-LRRK2 (αpSer1292 and αpSer935) and actin. (**B**). GFP, GFP-LRRK2 wildtype, kinase inactive [D2017A] or G2019S were expressed along with FLAG-p62 or p62 T138A in HEK293 cells. Cells were treated with the indicated concentrations of GNE1023 (0-3μM) for 90 minutes. Anti-FLAG immunoprecipitates were analyzed by pThr138 and p62 immunoblot. Cell lysates were probed for LRRK2 (αGFP and N241), phospho-LRRK2 (αpSer1292 and αpSer935) and actin.

Supplemental Figure 6. Primary rat embryonic cortical neurons were transfected on day four in vitro with un-tagged human LRRK2 (WT or G2019S) in pCMS-EGFP together with FLAG-tagged p62 (WT or T138A) at a ratio of 3:1 with LRRK2 in excess, as described [53]. Three days post-transfection, neurons were fixed and processed for anti-LRRK2 (c41-2) anti-FLAG/GFP immunofluorescence, with DAPI as a nuclear counterstain. (**A**) *Top panel*-Representative images of LRRK2 and p62 signals from LRRK2/p62 expression with normal nucleus. *Bottom panel*-representative image of LRRK2 [G2019S]/GFP signal with apoptotic neucleus. (**B&C**) Representative apoptotic nuclei from LRRK2 [G2019S]/p62 and LRRK2 [G2019S]/p62Thr138Ala, respectively.

Supplemental Figure 7. Further representative images of caspase-3 staining in LRRK2 and p62 co-transfected neurons as in **Figure 9**.

Literature Cited

1. Goedert, M., Spillantini, M. G., Del Tredici, K., and Braak, H. (2013) 100 years of Lewy pathology. *Nat Rev Neurol* **9**, 13-24
2. Spillantini, M. G., Schmidt, M. L., Lee, V. M., Trojanowski, J. Q., Jakes, R., and Goedert, M. (1997) Alpha-synuclein in Lewy bodies. *Nature* **388**, 839-840
3. Majcher, V., Goode, A., James, V., and Layfield, R. (2015) Autophagy receptor defects and ALS-FTLD. *Molecular and cellular neurosciences* **66**, 43-52
4. Watanabe, Y., Tatebe, H., Taguchi, K., Endo, Y., Tokuda, T., Mizuno, T., Nakagawa, M., and Tanaka, M. (2012) p62/SQSTM1-dependent autophagy of Lewy body-like alpha-synuclein inclusions. *PLoS One* **7**, e52868
5. Terni, B., Rey, M. J., Boluda, S., Torrejon-Escribano, B., Sabate, M. P., Calopa, M., van Leeuwen, F. W., and Ferrer, I. (2007) Mutant ubiquitin and p62 immunoreactivity in cases of combined multiple system atrophy and Alzheimer's disease. *Acta neuropathologica* **113**, 403-416
6. Gotzl, J. K., Lang, C. M., Haass, C., and Capell, A. (2016) Impaired protein degradation in FTLD and related disorders. *Ageing research reviews* **32**, 122-139
7. Joshi, G., Gan, K. A., Johnson, D. A., and Johnson, J. A. (2015) Increased Alzheimer's disease-like pathology in the APP/ PS1DeltaE9 mouse model lacking Nrf2 through modulation of autophagy. *Neurobiology of aging* **36**, 664-679
8. Zatloukal, K., Stumptner, C., Fuchsbichler, A., Heid, H., Schnoelzer, M., Kenner, L., Kleinert, R., Prinz, M., Aguzzi, A., and Denk, H. (2002) p62 Is a Common Component of Cytoplasmic Inclusions in Protein Aggregation Diseases. *The American Journal of Pathology* **160**, 255-263
9. Schulz-Schaeffer, W. J. (2010) The synaptic pathology of alpha-synuclein aggregation in dementia with Lewy bodies, Parkinson's disease and Parkinson's disease dementia. *Acta neuropathologica* **120**, 131-143
10. Kuusisto, E., Parkkinen, L., and Alafuzoff, I. (2003) Morphogenesis of Lewy bodies: dissimilar incorporation of alpha-synuclein, ubiquitin, and p62. *Journal of neuropathology and experimental neurology* **62**, 1241-1253
11. Kuusisto, E., Salminen, A., and Alafuzoff, I. (2001) Ubiquitin-binding protein p62 is present in neuronal and glial inclusions in human tauopathies and synucleinopathies. *Neuroreport* **12**, 2085-2090
12. Geetha, T., and Wooten, M. W. (2002) Structure and functional properties of the ubiquitin binding protein p62. *FEBS Lett* **512**, 19-24
13. Seibenhener, M. L., Du, Y., Diaz-Meco, M. T., Moscat, J., Wooten, M. C., and Wooten, M. W. (2013) A role for sequestosome 1/p62 in mitochondrial dynamics, import and genome integrity. *Biochim Biophys Acta* **1833**, 452-459
14. Lin, X., Li, S., Zhao, Y., Ma, X., Zhang, K., He, X., and Wang, Z. (2013) Interaction domains of p62: a bridge between p62 and selective autophagy. *DNA Cell Biol* **32**, 220-227
15. Moscat, J., Diaz-Meco, M. T., and Wooten, M. W. (2007) Signal integration and diversification through the p62 scaffold protein. *Trends Biochem Sci* **32**, 95-100
16. Moscat, J., Diaz-Meco, M. T., Albert, A., and Campuzano, S. (2006) Cell signaling and function organized by PB1 domain interactions. *Mol Cell* **23**, 631-640
17. Katsuragi, Y., Ichimura, Y., and Komatsu, M. (2015) p62/SQSTM1 functions as a signaling hub and an autophagy adaptor. *FEBS J* **282**, 4672-4678
18. Moscat, J., Karin, M., and Diaz-Meco, M. T. (2016) p62 in Cancer: Signaling Adaptor Beyond Autophagy. *Cell* **167**, 606-609
19. Ichimura, Y., Waguri, S., Sou, Y. S., Kageyama, S., Hasegawa, J., Ishimura, R., Saito, T., Yang, Y., Kouno, T., Fukutomi, T., Hoshii, T., Hirao, A., Takagi, K., Mizushima, T., Motohashi, H., Lee, M. S.,

Yoshimori, T., Tanaka, K., Yamamoto, M., and Komatsu, M. (2013) Phosphorylation of p62 activates the Keap1-Nrf2 pathway during selective autophagy. *Mol Cell* **51**, 618-631

20. Hashimoto, K., Simmons, A. N., Kajino-Sakamoto, R., Tsuji, Y., and Ninomiya-Tsuji, J. (2016) TAK1 Regulates the Nrf2 Antioxidant System Through Modulating p62/SQSTM1. *Antioxidants & redox signaling* **25**, 953-964
21. Watanabe, Y., Tsujimura, A., Taguchi, K., and Tanaka, M. (2017) HSF1 stress response pathway regulates autophagy receptor SQSTM1/p62-associated proteostasis. *Autophagy* **13**, 133-148
22. Matsumoto, G., Shimogori, T., Hattori, N., and Nukina, N. (2015) TBK1 controls autophagosomal engulfment of polyubiquitinated mitochondria through p62/SQSTM1 phosphorylation. *Hum Mol Genet* **24**, 4429-4442
23. Pilli, M., Arko-Mensah, J., Ponpuak, M., Roberts, E., Master, S., Mandell, M. A., Dupont, N., Ornatowski, W., Jiang, S., Bradfute, S. B., Bruun, J. A., Hansen, T. E., Johansen, T., and Deretic, V. (2012) TBK-1 promotes autophagy-mediated antimicrobial defense by controlling autophagosome maturation. *Immunity* **37**, 223-234
24. Matsumoto, G., Wada, K., Okuno, M., Kurosawa, M., and Nukina, N. (2011) Serine 403 phosphorylation of p62/SQSTM1 regulates selective autophagic clearance of ubiquitinated proteins. *Mol Cell* **44**, 279-289
25. Lim, J., Lachenmayer, M. L., Wu, S., Liu, W., Kundu, M., Wang, R., Komatsu, M., Oh, Y. J., Zhao, Y., and Yue, Z. (2015) Proteotoxic stress induces phosphorylation of p62/SQSTM1 by ULK1 to regulate selective autophagic clearance of protein aggregates. *PLoS Genet* **11**, e1004987
26. Linares, J. F., Amanchy, R., Greis, K., Diaz-Meco, M. T., and Moscat, J. (2011) Phosphorylation of p62 by cdk1 controls the timely transit of cells through mitosis and tumor cell proliferation. *Mol Cell Biol* **31**, 105-117
27. Linares, J. F., Duran, A., Reina-Campos, M., Aza-Blanc, P., Campos, A., Moscat, J., and Diaz-Meco, M. T. (2015) Amino Acid Activation of mTORC1 by a PB1-Domain-Driven Kinase Complex Cascade. *Cell reports* **12**, 1339-1352
28. Christian, F., Krause, E., Houslay, M. D., and Baillie, G. S. (2014) PKA phosphorylation of p62/SQSTM1 regulates PB1 domain interaction partner binding. *Biochim Biophys Acta* **1843**, 2765-2774
29. Berg, D., Schweitzer, K., Leitner, P., Zimprich, A., Lichtner, P., Belcredi, P., Brussel, T., Schulte, C., Maass, S., and Nagele, T. (2005) Type and frequency of mutations in the LRRK2 gene in familial and sporadic Parkinson's disease*. *Brain* **128**, 3000-3011
30. Zimprich, A., Biskup, S., Leitner, P., Lichtner, P., Farrer, M., Lincoln, S., Kachergus, J., Hulihan, M., Uitti, R. J., Calne, D. B., Stoessl, A. J., Pfeiffer, R. F., Patenge, N., Carbajal, I. C., Vieregge, P., Asmus, F., Muller-Myhsok, B., Dickson, D. W., Meitinger, T., Strom, T. M., Wszolek, Z. K., and Gasser, T. (2004) Mutations in LRRK2 cause autosomal-dominant parkinsonism with pleomorphic pathology. *Neuron* **44**, 601-607
31. Paisan-Ruiz, C., Jain, S., Evans, E. W., Gilks, W. P., Simon, J., van der Brug, M., Lopez de Munain, A., Aparicio, S., Gil, A. M., Khan, N., Johnson, J., Martinez, J. R., Nicholl, D., Carrera, I. M., Pena, A. S., de Silva, R., Lees, A., Marti-Masso, J. F., Perez-Tur, J., Wood, N. W., and Singleton, A. B. (2004) Cloning of the gene containing mutations that cause PARK8-linked Parkinson's disease. *Neuron* **44**, 595-600
32. Mata, I. F., Kachergus, J. M., Taylor, J. P., Lincoln, S., Aasly, J., Lynch, T., Hulihan, M. M., Cobb, S. A., Wu, R. M., Lu, C. S., Lahoz, C., Wszolek, Z. K., and Farrer, M. J. (2005) Lrrk2 pathogenic substitutions in Parkinson's disease. *Neurogenetics* **6**, 171-177
33. Di Fonzo, A., Rohe, C. F., Ferreira, J., Chien, H. F., Vacca, L., Stocchi, F., Guedes, L., Fabrizio, E., Manfredi, M., Vanacore, N., Goldwurm, S., Breedveld, G., Sampaio, C., Meco, G., Barbosa, E.,

Oostra, B. A., and Bonifati, V. (2005) A frequent LRRK2 gene mutation associated with autosomal dominant Parkinson's disease. *Lancet* **365**, 412-415

34. Di Fonzo, A., Tassorelli, C., De Mari, M., Chien, H. F., Ferreira, J., Rohe, C. F., Riboldazzi, G., Antonini, A., Albani, G., Mauro, A., Marconi, R., Abbruzzese, G., Lopiano, L., Fincati, E., Guidi, M., Marini, P., Stocchi, F., Onofrj, M., Toni, V., Tinazzi, M., Fabbrini, G., Lamberti, P., Vanacore, N., Meco, G., Leitner, P., Uitti, R. J., Wszolek, Z. K., Gasser, T., Simons, E. J., Breedveld, G. J., Goldwurm, S., Pezzoli, G., Sampaio, C., Barbosa, E., Martignoni, E., Oostra, B. A., and Bonifati, V. (2006) Comprehensive analysis of the LRRK2 gene in sixty families with Parkinson's disease. *Eur J Hum Genet* **14**, 322-331
35. Farrer, M., Stone, J., Mata, I. F., Lincoln, S., Kachergus, J., Hulihan, M., Strain, K. J., and Maraganore, D. M. (2005) LRRK2 mutations in Parkinson disease. *Neurology* **65**, 738-740
36. Healy, D. G., Falchi, M., O'Sullivan, S. S., Bonifati, V., Durr, A., Bressman, S., Brice, A., Aasly, J., Zabetian, C. P., Goldwurm, S., Ferreira, J. J., Tolosa, E., Kay, D. M., Klein, C., Williams, D. R., Marras, C., Lang, A. E., Wszolek, Z. K., Berciano, J., Schapira, A. H., Lynch, T., Bhatia, K. P., Gasser, T., Lees, A. J., and Wood, N. W. (2008) Phenotype, genotype, and worldwide genetic penetrance of LRRK2-associated Parkinson's disease: a case-control study. *Lancet Neurol* **7**, 583-590
37. Paisan-Ruiz, C., Nath, P., Washecka, N., Gibbs, J. R., and Singleton, A. B. (2008) Comprehensive analysis of LRRK2 in publicly available Parkinson's disease cases and neurologically normal controls. *Hum Mutat* **29**, 485-490
38. Skipper, L., Li, Y., Bonnard, C., Pavanni, R., Yih, Y., Chua, E., Sung, W. K., Tan, L., Wong, M. C., Tan, E. K., and Liu, J. (2005) Comprehensive evaluation of common genetic variation within LRRK2 reveals evidence for association with sporadic Parkinson's disease. *Hum Mol Genet* **14**, 3549-3556
39. Lesage, S., Patin, E., Condroyer, C., Leutenegger, A. L., Lohmann, E., Giladi, N., Bar-Shira, A., Belarbi, S., Hecham, N., Pollak, P., Ouvrard-Hernandez, A. M., Bardien, S., Carr, J., Benhassine, T., Tomiyama, H., Pirkevi, C., Hamadouche, T., Cazeneuve, C., Basak, A. N., Hattori, N., Durr, A., Tazir, M., Orr-Urtreger, A., Quintana-Murci, L., and Brice, A. (2010) Parkinson's disease-related LRRK2 G2019S mutation results from independent mutational events in humans. *Hum Mol Genet*
40. Greggio, E., and Cookson, M. R. (2009) Leucine Rich Repeat Kinase 2 mutations and Parkinson's disease: Three Questions. *ASN Neuro* **In Press**
41. West, A. B., Moore, D. J., Biskup, S., Bugayenko, A., Smith, W. W., Ross, C. A., Dawson, V. L., and Dawson, T. M. (2005) Parkinson's disease-associated mutations in leucine-rich repeat kinase 2 augment kinase activity. *Proc Natl Acad Sci U S A* **102**, 16842-16847
42. Jaleel, M., Nichols, R. J., Deak, M., Campbell, D. G., Gillardon, F., Knebel, A., and Alessi, D. R. (2007) LRRK2 phosphorylates moesin at threonine-558: characterization of how Parkinson's disease mutants affect kinase activity. *Biochem J* **405**, 307-317
43. Doggett, E. A., Zhao, J., Mork, C. N., Hu, D., and Nichols, R. J. (2012) Phosphorylation of LRRK2 serines 955 and 973 is disrupted by Parkinson's disease mutations and LRRK2 pharmacological inhibition. *J Neurochem* **120**, 37-45
44. Sheng, Z., Zhang, S., Bustos, D., Kleinheinz, T., Le Pichon, C. E., Dominguez, S. L., Solanoy, H. O., Drummond, J., Zhang, X., Ding, X., Cai, F., Song, Q., Li, X., Yue, Z., van der Brug, M. P., Burdick, D. J., Gunzner-Toste, J., Chen, H., Liu, X., Estrada, A. A., Sweeney, Z. K., Scearce-Levie, K., Moffat, J. G., Kirkpatrick, D. S., and Zhu, H. (2012) Ser1292 autophosphorylation is an indicator of LRRK2 kinase activity and contributes to the cellular effects of PD mutations. *Sci Transl Med* **4**, 164ra161
45. Alegre-Abarrategui, J., Christian, H., Lufino, M. M., Mutihac, R., Venda, L. L., Ansorge, O., and Wade-Martins, R. (2009) LRRK2 regulates autophagic activity and localizes to specific membrane

microdomains in a novel human genomic reporter cellular model. *Hum Mol Genet* **18**, 4022-4034

46. Gomez-Suaga, P., Luzon-Toro, B., Churamani, D., Zhang, L., Bloor-Young, D., Patel, S., Woodman, P. G., Churchill, G. C., and Hilfiker, S. (2012) Leucine-rich repeat kinase 2 regulates autophagy through a calcium-dependent pathway involving NAADP. *Hum Mol Genet* **21**, 511-525
47. Alegre-Abarrategui, J., Ansorge, O., Esiri, M., and Wade-Martins, R. (2008) LRRK2 is a component of granular alpha-synuclein pathology in the brainstem of Parkinson's disease. *Neuropathology and applied neurobiology* **34**, 272-283
48. Tong, Y., Yamaguchi, H., Giaime, E., Boyle, S., Kopan, R., Kelleher, R. J., 3rd, and Shen, J. (2010) Loss of leucine-rich repeat kinase 2 causes impairment of protein degradation pathways, accumulation of alpha-synuclein, and apoptotic cell death in aged mice. *Proc Natl Acad Sci U S A* **107**, 9879-9884
49. Hinkle, K. M., Yue, M., Behrouz, B., Dachsel, J. C., Lincoln, S. J., Bowles, E. E., Beevers, J. E., Dugger, B., Winner, B., Prots, I., Kent, C. B., Nishioka, K., Lin, W. L., Dickson, D. W., Janus, C. J., Farrer, M. J., and Melrose, H. L. (2012) LRRK2 knockout mice have an intact dopaminergic system but display alterations in exploratory and motor co-ordination behaviors. *Molecular neurodegeneration* **7**, 25
50. Cookson, M. R. (2017) Mechanisms of Mutant LRRK2 Neurodegeneration. *Adv Neurobiol* **14**, 227-239
51. Martin, I., Kim, J. W., Lee, B. D., Kang, H. C., Xu, J. C., Jia, H., Stankowski, J., Kim, M. S., Zhong, J., Kumar, M., Andrabi, S. A., Xiong, Y., Dickson, D. W., Wszolek, Z. K., Pandey, A., Dawson, T. M., and Dawson, V. L. (2014) Ribosomal protein s15 phosphorylation mediates LRRK2 neurodegeneration in Parkinson's disease. *Cell* **157**, 472-485
52. Imai, Y., Gehrke, S., Wang, H. Q., Takahashi, R., Hasegawa, K., Oota, E., and Lu, B. (2008) Phosphorylation of 4E-BP by LRRK2 affects the maintenance of dopaminergic neurons in Drosophila. *EMBO J* **27**, 2432-2443
53. Sanders, L. H., Laganiere, J., Cooper, O., Mak, S. K., Vu, B. J., Huang, Y. A., Paschon, D. E., Vangipuram, M., Sundararajan, R., Urnov, F. D., Langston, J. W., Gregory, P. D., Zhang, H. S., Greenamyre, J. T., Isacson, O., and Schule, B. (2014) LRRK2 mutations cause mitochondrial DNA damage in iPSC-derived neural cells from Parkinson's disease patients: reversal by gene correction. *Neurobiol Dis* **62**, 381-386
54. Hsieh, C. H., Shaltouki, A., Gonzalez, A. E., Bettencourt da Cruz, A., Burbulla, L. F., St Lawrence, E., Schule, B., Krainc, D., Palmer, T. D., and Wang, X. (2016) Functional Impairment in Miro Degradation and Mitophagy Is a Shared Feature in Familial and Sporadic Parkinson's Disease. *Cell Stem Cell* **19**, 709-724
55. Yue, M., Hinkle, K., Davies, P., Trushina, E., Fiesel, F., Christenson, T., Schroeder, A., Zhang, L., Bowles, E., Behrouz, B., Lincoln, S., Beevers, J., Milnerwood, A., Kurti, A., McLean, P. J., Fryer, J. D., Springer, W., Dickson, D., Farrer, M., and Melrose, H. (2015) Progressive dopaminergic alterations and mitochondrial abnormalities in LRRK2 G2019S knock in mice. *Neurobiol Dis*
56. Su, Y. C., and Qi, X. (2013) Inhibition of excessive mitochondrial fission reduced aberrant autophagy and neuronal damage caused by LRRK2 G2019S mutation. *Hum Mol Genet* **22**, 4545-4561
57. Abeliovich, A., and Gitler, A. D. (2016) Defects in trafficking bridge Parkinson's disease pathology and genetics. *Nature* **539**, 207-216
58. Steger, M., Tonelli, F., Ito, G., Davies, P., Trost, M., Vetter, M., Wachter, S., Lorentzen, E., Duddy, G., Wilson, S., Baptista, M. A., Fiske, B. K., Fell, M. J., Morrow, J. A., Reith, A. D., Alessi, D. R., and Mann, M. (2016) Phosphoproteomics reveals that Parkinson's disease kinase LRRK2 regulates a subset of Rab GTPases. *Elife* **5**

59. Alegre-Abarrategui, J., and Wade-Martins, R. (2009) Parkinson disease, LRRK2 and the endocytic-autophagic pathway. *Autophagy* **5**, 1208-1210
60. Plowey, E. D., Cherra, S. J., 3rd, Liu, Y. J., and Chu, C. T. (2008) Role of autophagy in G2019S-LRRK2-associated neurite shortening in differentiated SH-SY5Y cells. *J Neurochem* **105**, 1048-1056
61. Plowey, E. D., Johnson, J. W., Steer, E., Zhu, W., Eisenberg, D. A., Valentino, N. M., Liu, Y. J., and Chu, C. T. (2014) Mutant LRRK2 enhances glutamatergic synapse activity and evokes excitotoxic dendrite degeneration. *Biochim Biophys Acta* **1842**, 1596-1603
62. Park, S., Han, S., Choi, I., Kim, B., Park, S. P., Joe, E. H., and Suh, Y. H. (2016) Interplay between Leucine-Rich Repeat Kinase 2 (LRRK2) and p62/SQSTM-1 in Selective Autophagy. *PLoS One* **11**, e0163029
63. Schapansky, J., Nardozzi, J. D., Felizia, F., and LaVoie, M. J. (2014) Membrane recruitment of endogenous LRRK2 precedes its potent regulation of autophagy. *Hum Mol Genet* **23**, 4201-4214
64. Orenstein, S. J., Kuo, S. H., Tasset, I., Arias, E., Koga, H., Fernandez-Carasa, I., Cortes, E., Honig, L. S., Dauer, W., Consiglio, A., Raya, A., Sulzer, D., and Cuervo, A. M. (2013) Interplay of LRRK2 with chaperone-mediated autophagy. *Nat Neurosci* **16**, 394-406
65. Tong, Y., Giaime, E., Yamaguchi, H., Ichimura, T., Liu, Y., Si, H., Cai, H., Bonventre, J. V., and Shen, J. (2012) Loss of leucine-rich repeat kinase 2 causes age-dependent bi-phasic alterations of the autophagy pathway. *Molecular neurodegeneration* **7**, 2
66. Soukup, S. F., Kuenen, S., Vanhauwaert, R., Manetsberger, J., Hernandez-Diaz, S., Swerts, J., Schoovaerts, N., Vilain, S., Gounko, N. V., Vints, K., Geens, A., De Strooper, B., and Verstreken, P. (2016) A LRRK2-Dependent EndophilinA Phosphoswitch Is Critical for Macroautophagy at Presynaptic Terminals. *Neuron* **92**, 829-844
67. Law, B. M., Spain, V. A., Leinster, V. H., Chia, R., Beilina, A., Cho, H. J., Taymans, J. M., Urban, M. K., Sancho, R. M., Ramirez, M. B., Biskup, S., Baekelandt, V., Cai, H., Cookson, M. R., Berwick, D. C., and Harvey, K. (2014) A direct interaction between leucine-rich repeat kinase 2 and specific beta-tubulin isoforms regulates tubulin acetylation. *J Biol Chem* **289**, 895-908
68. Caesar, M., Zach, S., Carlson, C. B., Brockmann, K., Gasser, T., and Gillardon, F. (2013) Leucine-rich repeat kinase 2 functionally interacts with microtubules and kinase-dependently modulates cell migration. *Neurobiol Dis* **54**, 280-288
69. Kett, L. R., Boassa, D., Ho, C. C., Rideout, H. J., Hu, J., Terada, M., Ellisman, M., and Dauer, W. T. (2012) LRRK2 Parkinson disease mutations enhance its microtubule association. *Hum Mol Genet* **21**, 890-899
70. Bailey, R. M., Covy, J. P., Melrose, H. L., Rousseau, L., Watkinson, R., Knight, J., Miles, S., Farrer, M. J., Dickson, D. W., Giasson, B. I., and Lewis, J. (2013) LRRK2 phosphorylates novel tau epitopes and promotes tauopathy. *Acta neuropathologica* **126**, 809-827
71. Kawakami, F., Yabata, T., Ohta, E., Maekawa, T., Shimada, N., Suzuki, M., Maruyama, H., Ichikawa, T., and Obata, F. (2012) LRRK2 phosphorylates tubulin-associated tau but not the free molecule: LRRK2-mediated regulation of the tau-tubulin association and neurite outgrowth. *PLoS One* **7**, e30834
72. Parisiadou, L., Xie, C., Cho, H. J., Lin, X., Gu, X. L., Long, C. X., Lobbestael, E., Baekelandt, V., Taymans, J. M., Sun, L., and Cai, H. (2009) Phosphorylation of ezrin/radixin/moesin proteins by LRRK2 promotes the rearrangement of actin cytoskeleton in neuronal morphogenesis. *J Neurosci* **29**, 13971-13980
73. Berwick, D. C., and Harvey, K. (2012) LRRK2 functions as a Wnt signaling scaffold, bridging cytosolic proteins and membrane-localized LRP6. *Hum Mol Genet* **21**, 4966-4979
74. Sancho, R. M., Law, B. M., and Harvey, K. (2009) Mutations in the LRRK2 Roc-COR tandem domain link Parkinson's disease to Wnt signalling pathways. *Hum Mol Genet* **18**, 3955-3968

75. Liu, Z., Lee, J., Krummey, S., Lu, W., Cai, H., and Lenardo, M. J. (2011) The kinase LRRK2 is a regulator of the transcription factor NFAT that modulates the severity of inflammatory bowel disease. *Nat Immunol* **12**, 1063-1070
76. Manzoni, C., Mamais, A., Roosen, D. A., Dihanich, S., Soutar, M. P., Plun-Favreau, H., Bandopadhyay, R., Hardy, J., Tooze, S. A., Cookson, M. R., and Lewis, P. A. (2016) mTOR independent regulation of macroautophagy by Leucine Rich Repeat Kinase 2 via Beclin-1. *Sci Rep* **6**, 35106
77. Manzoni, C., Mamais, A., Dihanich, S., Abeti, R., Soutar, M. P., Plun-Favreau, H., Giunti, P., Tooze, S. A., Bandopadhyay, R., and Lewis, P. A. (2013) Inhibition of LRRK2 kinase activity stimulates macroautophagy. *Biochim Biophys Acta* **1833**, 2900-2910
78. Saez-Atienzar, S., Bonet-Ponce, L., Blesa, J. R., Romero, F. J., Murphy, M. P., Jordan, J., and Galindo, M. F. (2014) The LRRK2 inhibitor GSK2578215A induces protective autophagy in SH-SY5Y cells: involvement of Drp-1-mediated mitochondrial fission and mitochondrial-derived ROS signaling. *Cell death & disease* **5**, e1368
79. Skibinski, G., Hwang, V., Ando, D. M., Daub, A., Lee, A. K., Ravisankar, A., Modan, S., Finucane, M. M., Shaby, B. A., and Finkbeiner, S. (2017) Nrf2 mitigates LRRK2- and alpha-synuclein-induced neurodegeneration by modulating proteostasis. *Proc Natl Acad Sci U S A* **114**, 1165-1170
80. Jiang, T., Harder, B., Rojo de la Vega, M., Wong, P. K., Chapman, E., and Zhang, D. D. (2015) p62 links autophagy and Nrf2 signaling. *Free radical biology & medicine* **88**, 199-204
81. Lobbestael, E., Zhao, J., Rudenko, I. N., Beylina, A., Gao, F., Wetter, J., Beullens, M., Bollen, M., Cookson, M. R., Baekelandt, V., Nichols, R. J., and Taymans, J. M. (2013) Identification of protein phosphatase 1 as a regulator of the LRRK2 phosphorylation cycle. *Biochem J* **456**, 119-128
82. Henderson, J. L., Kormos, B. L., Hayward, M. M., Coffman, K. J., Jasti, J., Kurumbail, R. G., Wager, T. T., Verhoest, P. R., Noell, G. S., Chen, Y., Needle, E., Berger, Z., Steyn, S. J., Houle, C., Hirst, W. D., and Galatsis, P. (2015) Discovery and preclinical profiling of 3-[4-(morpholin-4-yl)-7H-pyrrolo[2,3-d]pyrimidin-5-yl]benzonitrile (PF-06447475), a highly potent, selective, brain penetrant, and in vivo active LRRK2 kinase inhibitor. *J Med Chem* **58**, 419-432
83. Fell, M. J., Mirescu, C., Basu, K., Cheewatrakoolpong, B., DeMong, D. E., Ellis, J. M., Hyde, L. A., Lin, Y., Markgraf, C. G., Mei, H., Miller, M., Poulet, F. M., Scott, J. D., Smith, M. D., Yin, Z., Zhou, X., Parker, E. M., Kennedy, M. E., and Morrow, J. A. (2015) MLi-2, a Potent, Selective, and Centrally Active Compound for Exploring the Therapeutic Potential and Safety of LRRK2 Kinase Inhibition. *J Pharmacol Exp Ther* **355**, 397-409
84. Reed, S. E., Staley, E. M., Mayginnes, J. P., Pintel, D. J., and Tullis, G. E. (2006) Transfection of mammalian cells using linear polyethylenimine is a simple and effective means of producing recombinant adeno-associated virus vectors. *J Virol Methods* **138**, 85-98
85. Melachroinou, K., Leandrou, E., Valkimadi, P. E., Memou, A., Hadjigeorgiou, G., Stefanis, L., and Rideout, H. J. (2016) Activation of FADD-Dependent Neuronal Death Pathways as a Predictor of Pathogenicity for LRRK2 Mutations. *PLoS One* **11**, e0166053
86. Wang, L., Xie, C., Greggio, E., Parisiadou, L., Shim, H., Sun, L., Chandran, J., Lin, X., Lai, C., Yang, W. J., Moore, D. J., Dawson, T. M., Dawson, V. L., Chiosis, G., Cookson, M. R., and Cai, H. (2008) The chaperone activity of heat shock protein 90 is critical for maintaining the stability of leucine-rich repeat kinase 2. *J Neurosci* **28**, 3384-3391
87. Ding, X., and Goldberg, M. S. (2009) Regulation of LRRK2 stability by the E3 ubiquitin ligase CHIP. *PLoS One* **4**, e5949
88. Nichols, R. J., Dzamko, N., Morrice, N. A., Campbell, D. G., Deak, M., Ordureau, A., Macartney, T., Tong, Y., Shen, J., Prescott, A. R., and Alessi, D. R. (2010) 14-3-3 binding to LRRK2 is disrupted by multiple Parkinson's disease-associated mutations and regulates cytoplasmic localization. *Biochem J* **430**, 393-404

89. Toyofuku, T., Morimoto, K., Sasawatari, S., and Kumanogoh, A. (2015) Leucine-Rich Repeat Kinase 1 Regulates Autophagy through Turning On TBC1D2-Dependent Rab7 Inactivation. *Mol Cell Biol* **35**, 3044-3058
90. Reynolds, A., Doggett, E. A., Riddle, S. M., Lebakken, C. S., and Nichols, R. J. (2014) LRRK2 kinase activity and biology are not uniformly predicted by its autophosphorylation and cellular phosphorylation site status. *Frontiers in molecular neuroscience* **7**, 54
91. Nichols, R. J., Dzamko, N., Hutti, J. E., Cantley, L. C., Deak, M., Moran, J., Bamborough, P., Reith, A. D., and Alessi, D. R. (2009) Substrate specificity and inhibitors of LRRK2, a protein kinase mutated in Parkinson's disease. *Biochem J* **424**, 47-60
92. Ito, G., Katsemonova, K., Tonelli, F., Lis, P., Baptista, M. A., Shpiro, N., Duddy, G., Wilson, S., Ho, P. W., Ho, S. L., Reith, A. D., and Alessi, D. R. (2016) Phos-tag analysis of Rab10 phosphorylation by LRRK2: a powerful assay for assessing kinase function and inhibitors. *Biochem J* **473**, 2671-2685
93. Seibenhener, M. L., Babu, J. R., Geetha, T., Wong, H. C., Krishna, N. R., and Wooten, M. W. (2004) Sequestosome 1/p62 is a polyubiquitin chain binding protein involved in ubiquitin proteasome degradation. *Mol Cell Biol* **24**, 8055-8068
94. West, A. B., Moore, D. J., Choi, C., Andrabi, S. A., Li, X., Dikeman, D., Biskup, S., Zhang, Z., Lim, K. L., Dawson, V. L., and Dawson, T. M. (2007) Parkinson's disease-associated mutations in LRRK2 link enhanced GTP-binding and kinase activities to neuronal toxicity. *Hum Mol Genet* **16**, 223-232
95. Smith, W. W., Pei, Z., Jiang, H., Dawson, V. L., Dawson, T. M., and Ross, C. A. (2006) Kinase activity of mutant LRRK2 mediates neuronal toxicity. *Nat Neurosci* **9**, 1231-1233
96. Biosa, A., Trancikova, A., Civiero, L., Glauser, L., Bubacco, L., Greggio, E., and Moore, D. J. (2013) GTPase activity regulates kinase activity and cellular phenotypes of Parkinson's disease-associated LRRK2. *Hum Mol Genet* **22**, 1140-1156
97. Stafa, K., Trancikova, A., Webber, P. J., Glauser, L., West, A. B., and Moore, D. J. (2012) GTPase activity and neuronal toxicity of Parkinson's disease-associated LRRK2 is regulated by ArfGAP1. *PLoS Genet* **8**, e1002526
98. Greggio, E., Jain, S., Kingsbury, A., Bandopadhyay, R., Lewis, P., Kaganovich, A., van der Brug, M. P., Beilina, A., Blackinton, J., Thomas, K. J., Ahmad, R., Miller, D. W., Kesavapany, S., Singleton, A., Lees, A., Harvey, R. J., Harvey, K., and Cookson, M. R. (2006) Kinase activity is required for the toxic effects of mutant LRRK2/dardarin. *Neurobiol Dis* **23**, 329-341
99. Thirstrup, K., Dachsel, J. C., Oppermann, F. S., Williamson, D. S., Smith, G. P., Fog, K., and Christensen, K. V. (2017) Selective LRRK2 kinase inhibition reduces phosphorylation of endogenous Rab10 and Rab12 in human peripheral mononuclear blood cells. *Sci Rep* **7**, 10300
100. Arrigo, A. P. (2017) Mammalian HspB1 (Hsp27) is a molecular sensor linked to the physiology and environment of the cell. *Cell Stress Chaperones* **22**, 517-529
101. Carra, S., Alberti, S., Arrigo, P. A., Benesch, J. L., Benjamin, I. J., Boelens, W., Bartelt-Kirbach, B., Brundel, B., Buchner, J., Bukau, B., Carver, J. A., Ecroyd, H., Emanuelsson, C., Finet, S., Golenhofen, N., Goloubinoff, P., Gusev, N., Haslbeck, M., Hightower, L. E., Kampinga, H. H., Klevit, R. E., Liberek, K., McHaourab, H. S., McMenimen, K. A., Poletti, A., Quinlan, R., Strelkov, S. V., Toth, M. E., Vierling, E., and Tanguay, R. M. (2017) The growing world of small heat shock proteins: from structure to functions. *Cell Stress Chaperones* **22**, 601-611
102. Rudenko, I. N., Kaganovich, A., Langston, R. G., Beilina, A., Ndukwe, K., Kumaran, R., Dillman, A. A., Chia, R., and Cookson, M. R. (2017) The G2385R risk factor for Parkinson's disease enhances CHIP-dependent intracellular degradation of LRRK2. *Biochem J* **474**, 1547-1558

103. Rudenko, I. N., Kaganovich, A., Hauser, D. N., Beylina, A., Chia, R., Ding, J., Maric, D., Jaffe, H., and Cookson, M. R. (2012) The G2385R variant of leucine-rich repeat kinase 2 associated with Parkinson's disease is a partial loss-of-function mutation. *Biochem J* **446**, 99-111
104. Narayan, M., Zhang, J., Braswell, K., Gibson, C., Zitnyar, A., Lee, D. C., Varghese-Gupta, S., and Jinwal, U. K. (2015) Withaferin A Regulates LRRK2 Levels by Interfering with the Hsp90- Cdc37 Chaperone Complex. *Curr Aging Sci* **8**, 259-265
105. Ko, H. S., Bailey, R., Smith, W. W., Liu, Z., Shin, J. H., Lee, Y. I., Zhang, Y. J., Jiang, H., Ross, C. A., Moore, D. J., Patterson, C., Petrucelli, L., Dawson, T. M., and Dawson, V. L. (2009) CHIP regulates leucine-rich repeat kinase-2 ubiquitination, degradation, and toxicity. *Proc Natl Acad Sci U S A* **106**, 2897-2902
106. Godena, V. K., Brookes-Hocking, N., Moller, A., Shaw, G., Oswald, M., Sancho, R. M., Miller, C. C., Whitworth, A. J., and De Vos, K. J. (2014) Increasing microtubule acetylation rescues axonal transport and locomotor deficits caused by LRRK2 Roc-COR domain mutations. *Nature communications* **5**, 5245
107. Vitari, A. C., Thastrup, J., Rafiqi, F. H., Deak, M., Morrice, N. A., Karlsson, H. K., and Alessi, D. R. (2006) Functional interactions of the SPAK/OSR1 kinases with their upstream activator WNK1 and downstream substrate NKCC1. *Biochem J* **397**, 223-231
108. Mertins, P., Qiao, J. W., Patel, J., Udeshi, N. D., Clauser, K. R., Mani, D. R., Burgess, M. W., Gillette, M. A., Jaffe, J. D., and Carr, S. A. (2013) Integrated proteomic analysis of post-translational modifications by serial enrichment. *Nat Methods* **10**, 634-637
109. Wagner, S. A., Beli, P., Weinert, B. T., Scholz, C., Kelstrup, C. D., Young, C., Nielsen, M. L., Olsen, J. V., Brakebusch, C., and Choudhary, C. (2012) Proteomic analyses reveal divergent ubiquitylation site patterns in murine tissues. *Mol Cell Proteomics* **11**, 1578-1585
110. Kim, W., Bennett, E. J., Huttlin, E. L., Guo, A., Li, J., Possemato, A., Sowa, M. E., Rad, R., Rush, J., Comb, M. J., Harper, J. W., and Gygi, S. P. (2011) Systematic and quantitative assessment of the ubiquitin-modified proteome. *Mol Cell* **44**, 325-340
111. Hornbeck, P. V., Zhang, B., Murray, B., Kornhauser, J. M., Latham, V., and Skrzypek, E. (2015) PhosphoSitePlus, 2014: mutations, PTMs and recalibrations. *Nucleic Acids Res* **43**, D512-520
112. Athanasopoulos, P. S., Jacob, W., Neumann, S., Kutsch, M., Wolters, D., Tan, E. K., Bichler, Z., Hermann, C., and Heumann, R. (2016) Identification of protein phosphatase 2A as an interacting protein of leucine-rich repeat kinase 2. *Biol Chem*
113. Guaitoli, G., Raimondi, F., Gilsbach, B. K., Gomez-Llorente, Y., Deyaert, E., Renzi, F., Li, X., Schaffner, A., Jagtap, P. K., Boldt, K., von Zweydorf, F., Gotthardt, K., Lorimer, D. D., Yue, Z., Burgin, A., Janjic, N., Sattler, M., Versees, W., Ueffing, M., Ubarretxena-Belandia, I., Kortholt, A., and Gloeckner, C. J. (2016) Structural model of the dimeric Parkinson's protein LRRK2 reveals a compact architecture involving distant interdomain contacts. *Proc Natl Acad Sci U S A* **113**, E4357-4366
114. Gilsbach, B. K., Ho, F. Y., Vetter, I. R., van Haastert, P. J., Wittinghofer, A., and Kortholt, A. (2012) Roco kinase structures give insights into the mechanism of Parkinson disease-related leucine-rich-repeat kinase 2 mutations. *Proc Natl Acad Sci U S A* **109**, 10322-10327
115. Gotthardt, K., Weyand, M., Kortholt, A., Van Haastert, P. J., and Wittinghofer, A. (2008) Structure of the Roc-COR domain tandem of C. tepidum, a prokaryotic homologue of the human LRRK2 Parkinson kinase. *EMBO J* **27**, 2352
116. Sacino, A. N., Brooks, M., McKinney, A. B., Thomas, M. A., Shaw, G., Golde, T. E., and Giasson, B. I. (2014) Brain injection of alpha-synuclein induces multiple proteinopathies, gliosis, and a neuronal injury marker. *J Neurosci* **34**, 12368-12378

117. Tanji, K., Odagiri, S., Miki, Y., Maruyama, A., Nikaido, Y., Mimura, J., Mori, F., Warabi, E., Yanagawa, T., Ueno, S., Itoh, K., and Wakabayashi, K. (2015) p62 Deficiency Enhances alpha-Synuclein Pathology in Mice. *Brain Pathol* **25**, 552-564
118. Seibenhener, M. L., Geetha, T., and Wooten, M. W. (2007) Sequestosome 1/p62--more than just a scaffold. *FEBS Lett* **581**, 175-179
119. Bang, Y., Kim, K. S., Seol, W., and Choi, H. J. (2016) LRRK2 interferes with aggresome formation for autophagic clearance. *Molecular and cellular neurosciences* **75**, 71-80
120. Yang, S., Xia, C., Li, S., Du, L., Zhang, L., and Hu, Y. (2014) Mitochondrial dysfunction driven by the LRRK2-mediated pathway is associated with loss of Purkinje cells and motor coordination deficits in diabetic rat model. *Cell death & disease* **5**, e1217
121. Filimonenko, M., Stuffers, S., Raiborg, C., Yamamoto, A., Malerod, L., Fisher, E. M., Isaacs, A., Brech, A., Stenmark, H., and Simonsen, A. (2007) Functional multivesicular bodies are required for autophagic clearance of protein aggregates associated with neurodegenerative disease. *J Cell Biol* **179**, 485-500
122. Roosen, D. A., and Cookson, M. R. (2016) LRRK2 at the interface of autophagosomes, endosomes and lysosomes. *Molecular neurodegeneration* **11**, 73
123. Cookson, M. R. (2015) LRRK2 Pathways Leading to Neurodegeneration. *Curr Neurol Neurosci Rep* **15**, 42
124. Beilina, A., Rudenko, I. N., Kaganovich, A., Civiero, L., Chau, H., Kalia, S. K., Kalia, L. V., Lobbestael, E., Chia, R., Ndukwe, K., Ding, J., Nalls, M. A., International Parkinson's Disease Genomics, C., North American Brain Expression, C., Olszewski, M., Hauser, D. N., Kumaran, R., Lozano, A. M., Baekelandt, V., Greene, L. E., Taymans, J. M., Greggio, E., and Cookson, M. R. (2014) Unbiased screen for interactors of leucine-rich repeat kinase 2 supports a common pathway for sporadic and familial Parkinson disease. *Proc Natl Acad Sci U S A* **111**, 2626-2631
125. Berger, Z., Smith, K. A., and Lavoie, M. J. (2010) Membrane localization of LRRK2 is associated with increased formation of the highly active LRRK2 dimer and changes in its phosphorylation. *Biochemistry* **49**, 5511-5523
126. Ugun-Klusek, A., Tatham, M. H., Elkharaz, J., Constantin-Teodosiu, D., Lawler, K., Mohamed, H., Paine, S. M., Anderson, G., John Mayer, R., Lowe, J., Ellen Billett, E., and Bedford, L. (2017) Continued 26S proteasome dysfunction in mouse brain cortical neurons impairs autophagy and the Keap1-Nrf2 oxidative defence pathway. *Cell death & disease* **8**, e2531
127. Ran, F. A., Hsu, P. D., Wright, J., Agarwala, V., Scott, D. A., and Zhang, F. (2013) Genome engineering using the CRISPR-Cas9 system. *Nat Protoc* **8**, 2281-2308
128. Liu, J., Lee, W., Jiang, Z., Chen, Z., Jhunjhunwala, S., Haverty, P. M., Gnad, F., Guan, Y., Gilbert, H. N., Stinson, J., Klijn, C., Guillory, J., Bhatt, D., Vartanian, S., Walter, K., Chan, J., Holcomb, T., Dijkgraaf, P., Johnson, S., Koeman, J., Minna, J. D., Gazdar, A. F., Stern, H. M., Hoeflich, K. P., Wu, T. D., Settleman, J., de Sauvage, F. J., Gentleman, R. C., Neve, R. M., Stokoe, D., Modrusan, Z., Seshagiri, S., Shames, D. S., and Zhang, Z. (2012) Genome and transcriptome sequencing of lung cancers reveal diverse mutational and splicing events. *Genome Res* **22**, 2315-2327
129. Beausoleil, S. A., Villen, J., Gerber, S. A., Rush, J., and Gygi, S. P. (2006) A probability-based approach for high-throughput protein phosphorylation analysis and site localization. *Nat Biotechnol* **24**, 1285-1292

Figure 1

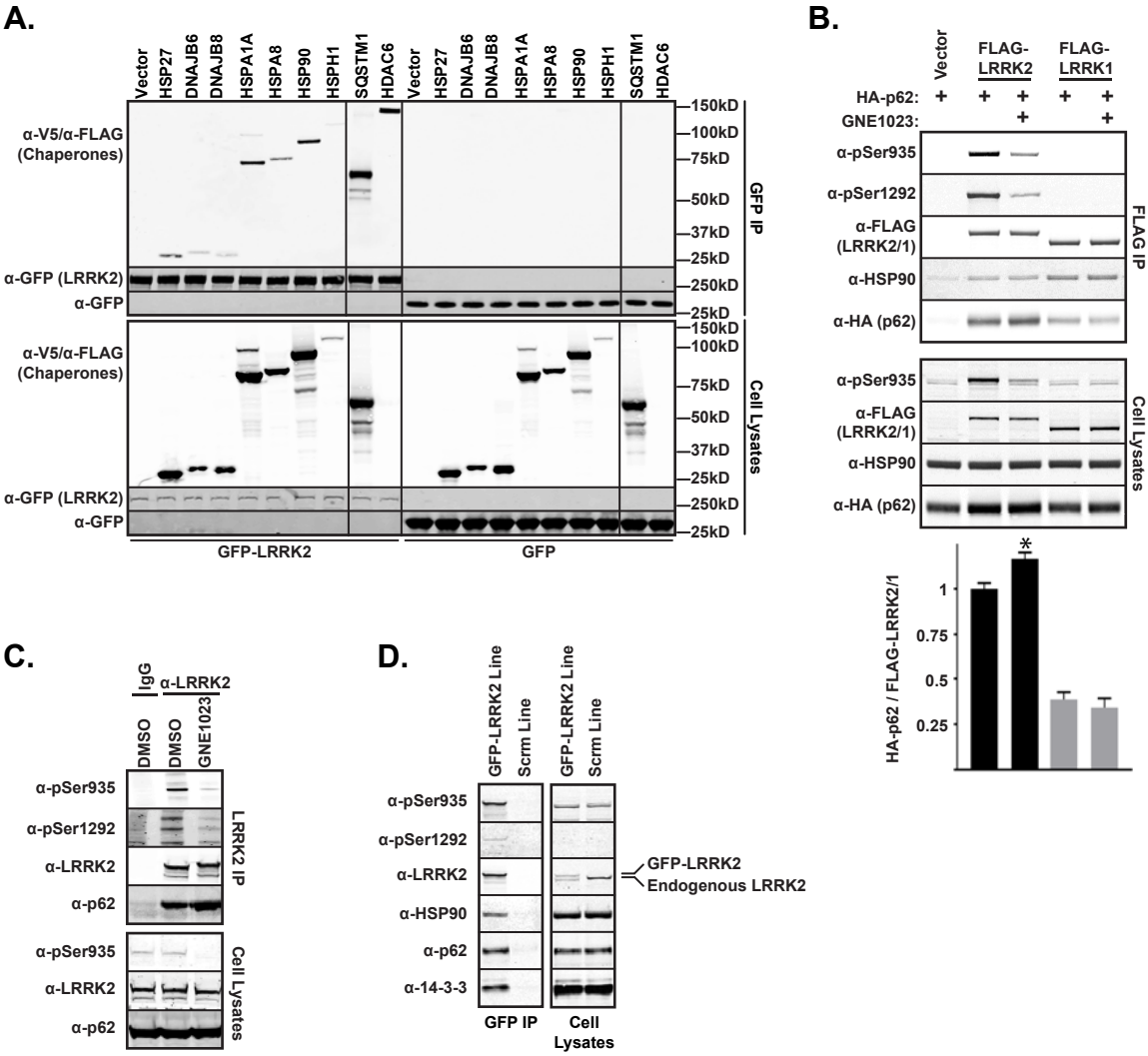
A.
Vector
HSP27
DNAJB6
DNAJB8
HSPA1A
HSPA8
HSP90
HSPH1
SQSTM1
HDAC6
α-V5/α-FLAG (Chaperones)
α-GFP (LRRK2)
α-GFP
150kD
100kD
75kD
50kD
37kD
25kD
250kD
GFP IP
Cell Lysates
GFP-LRRK2
GFP
B.
Vector
FLAG-LRRK2
FLAG-LRRK1
HA-p62:
GNE1023:
α-pSer935
α-pSer1292
α-FLAG (LRRK2/1)
α-HSP90
α-HA (p62)
FLAG IP
Cell Lysates
HA-p62 / FLAG-LRRK2/1
1
0.75
0.5
0.25
*
C.
IgG
α-LRRK2
DMSO
DMSO
GNE1023
α-pSer935
α-pSer1292
α-LRRK2
α-p62
LRRK2 IP
Cell Lysates
D.
GFP-LRRK2 Line
Scrm Line
α-pSer935
α-pSer1292
α-LRRK2
α-HSP90
α-p62
α-14-3-3
GFP-LRRK2
Endogenous LRRK2
GFP IP
Cell Lysates

Figure 2

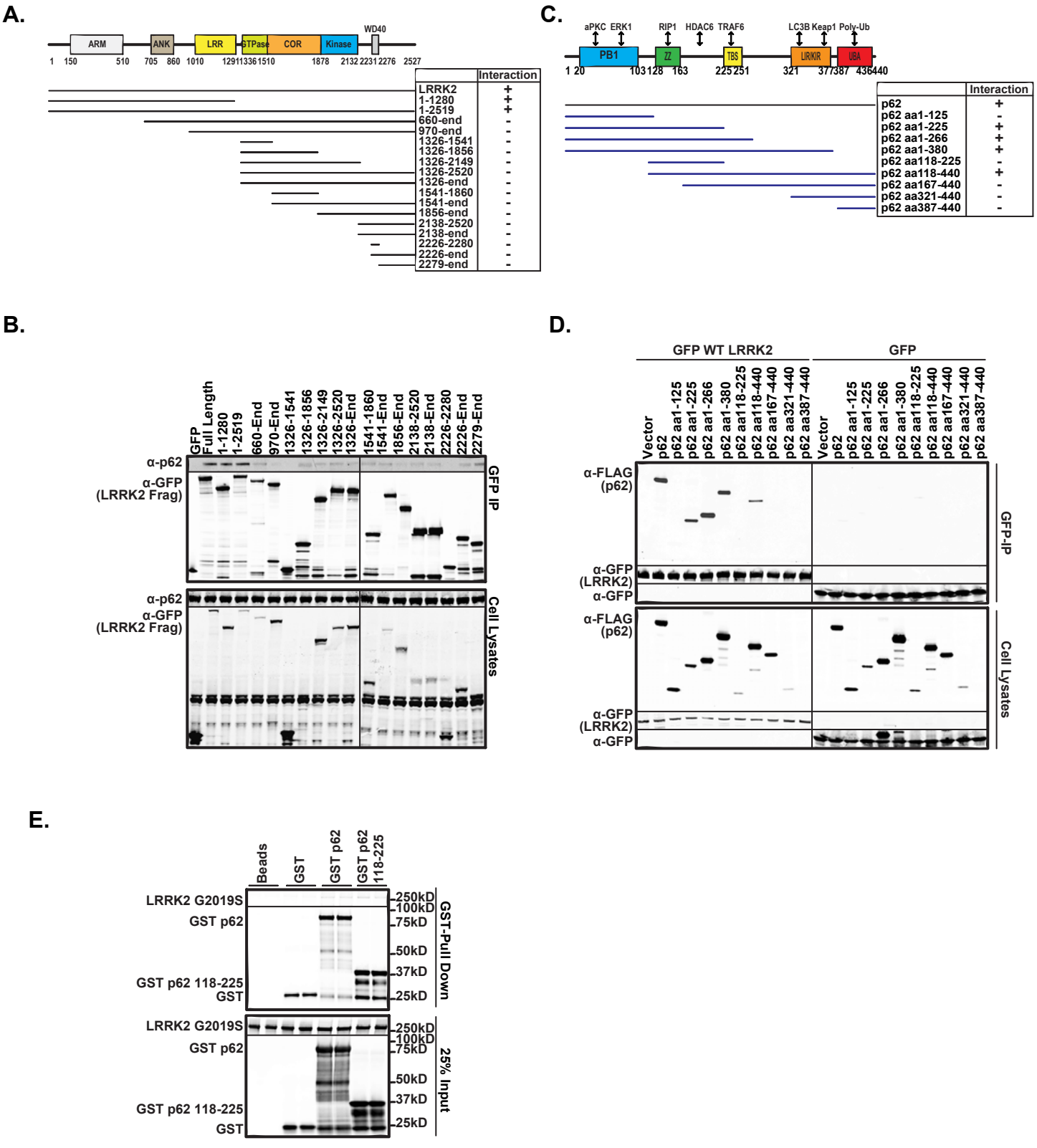
A.
ARM
ANK
LRR
GTPase
COR
Kinase
WD40
1 150 510 705 860 1010 1291 1336 1510 1878 2132 2231 2276 2527
Interaction
LRRK2 +
1-1280 +
1-2519 +
660-end -
970-end -
1326-1541 -
1326-1856 -
1326-2149 -
1326-2520 -
1326-end -
1541-1860 -
1541-end -
1856-end -
2138-2520 -
2138-end -
2226-2280 -
2226-end -
2279-end -
C.
aPKC ERK1
RIP1 HDAC6 TRAF6
LC3B Keap1 Poly-Ub
PB1
ZZ
TBS
LIR/KIR
UBA
1 20 103 128 163 225 251 321 377 387 436 440
Interaction
p62 +
p62 aa1-125 -
p62 aa1-225 +
p62 aa1-266 +
p62 aa1-380 +
p62 aa118-225 -
p62 aa118-440 +
p62 aa167-440 -
p62 aa321-440 -
p62 aa387-440 -
B.
GFP
Full Length
1-1280
1-2519
660-End
970-End
1326-1541
1326-1856
1326-2149
1326-2520
1326-End
1541-1860
1541-End
1856-End
2138-2520
2138-End
2226-2280
2226-End
2279-End
α-p62
α-GFP (LRRK2 Frag)
GFP IP
α-p62
α-GFP (LRRK2 Frag)
Cell Lysates
D.
GFP WT LRRK2
GFP
Vector
p62
p62 aa1-125
p62 aa1-225
p62 aa1-266
p62 aa1-380
p62 aa118-225
p62 aa118-440
p62 aa167-440
p62 aa321-440
p62 aa387-440
α-FLAG (p62)
α-GFP (LRRK2)
α-GFP
GFP-IP
Cell Lysates
E.
Beads
GST
GST p62
GST p62 118-225
LRRK2 G2019S
GST p62
GST p62 118-225
GST
250kD
100kD
75kD
50kD
37kD
25kD
GST-Pull Down
25% Input

Figure 3

A.

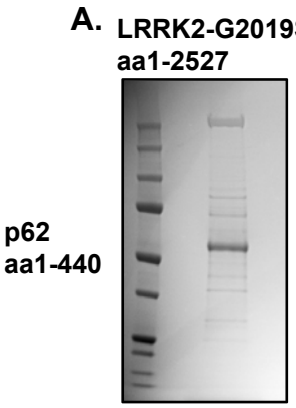

Site (WT)	Modifica on	Best Ascore	Localiza on Probability	Total SpC
S88	Phospho	30.97	1.000	2
T138	Phospho	1,000.00	1.000	25
T164	Phospho	224.33	1.000	6
S176	Phospho	1,000.00	1.000	10
S180	Phospho	21.95	0.994	1
S266	Phospho	26.2	0.997	1
T269	Phospho	16.24	0.977	3
Y383	Phospho	56.46	1.000	1
T430	Phospho	26.2	1.000	1

B.

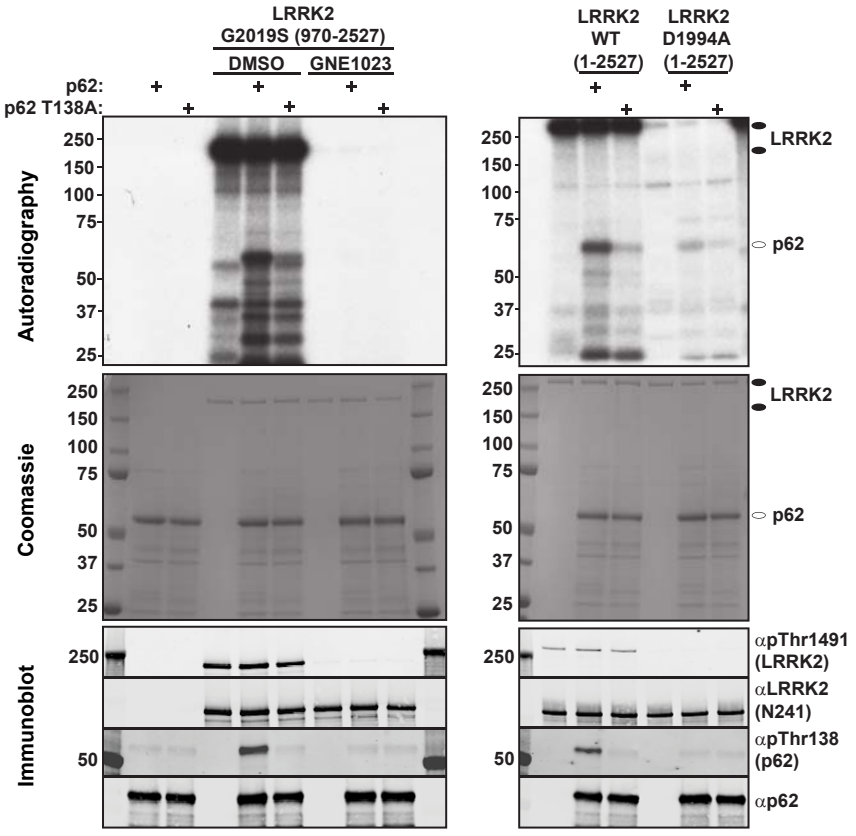

Figure 4

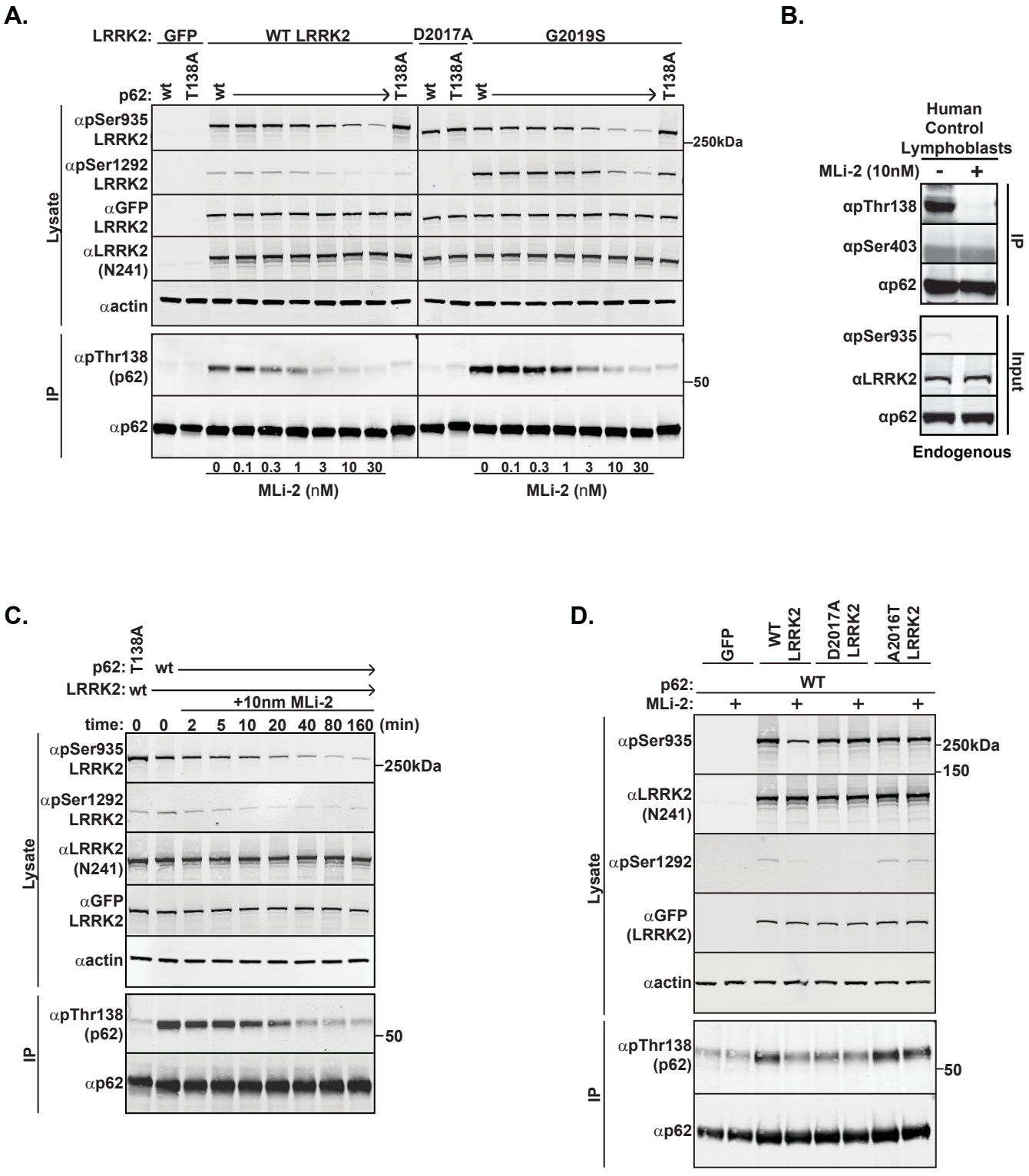
A.
LRRK2: GFP
WT LRRK2
D2017A
G2019S
p62: wt
T138A
wt
T138A
wt
T138A
wt
T138A
αpSer935 LRRK2
αpSer1292 LRRK2
αGFP LRRK2
αLRRK2 (N241)
αactin
Lysate
250kDa
αpThr138 (p62)
αp62
IP
50
0 0.1 0.3 1 3 10 30
MLi-2 (nM)
0 0.1 0.3 1 3 10 30
MLi-2 (nM)
B.
Human Control Lymphoblasts
MLi-2 (10nM) - +
αpThr138
αpSer403
αp62
IP
αpSer935
αLRRK2
αp62
Input
Endogenous
C.
p62: T138A
wt
LRRK2: wt
+10nm MLi-2
time: 0 0 2 5 10 20 40 80 160 (min)
αpSer935 LRRK2
αpSer1292 LRRK2
αLRRK2 (N241)
αGFP LRRK2
αactin
Lysate
250kDa
αpThr138 (p62)
αp62
IP
50
D.
GFP
WT LRRK2
D2017A LRRK2
A2016T LRRK2
p62: WT
MLi-2: + + + +
αpSer935
αLRRK2 (N241)
αpSer1292
αGFP (LRRK2)
αactin
Lysate
250kDa
150
αpThr138 (p62)
αp62
IP
50

Figure 5

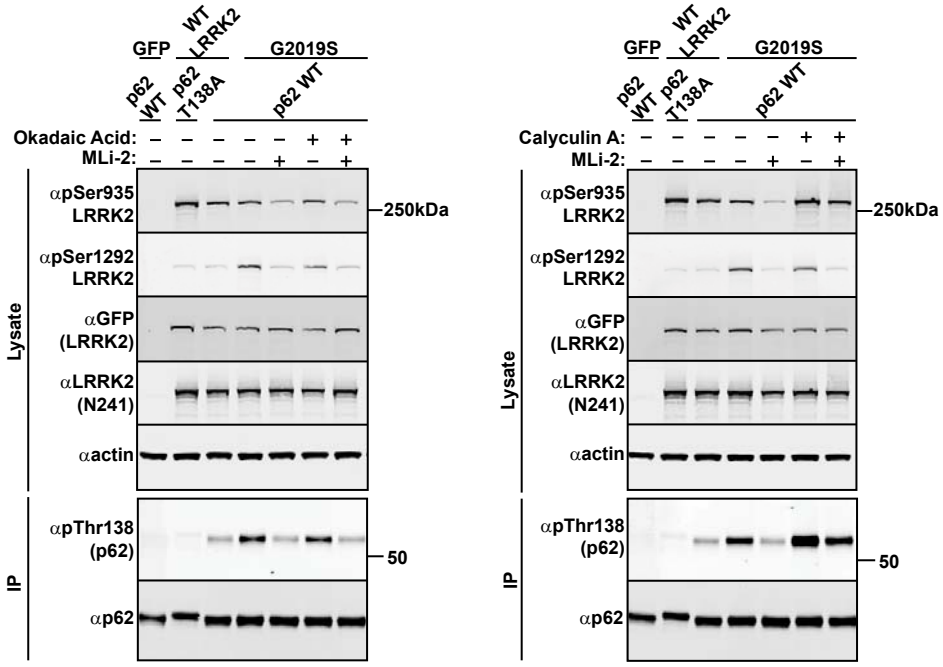
GFP
WT LRRK2
G2019S
p62 WT
p62 T138A
p62 WT
Okadaic Acid: – – – – – + +
MLi-2: – – – – + – +
Lysate
αpSer935 LRRK2
αpSer1292 LRRK2
αGFP (LRRK2)
αLRRK2 (N241)
αactin
250kDa
IP
αpThr138 (p62)
αp62
50
GFP
WT LRRK2
G2019S
p62 WT
p62 T138A
p62 WT
Calyculin A: – – – – – + +
MLi-2: – – – – + – +
Lysate
αpSer935 LRRK2
αpSer1292 LRRK2
αGFP (LRRK2)
αLRRK2 (N241)
αactin
250kDa
IP
αpThr138 (p62)
αp62
50

Figure 6

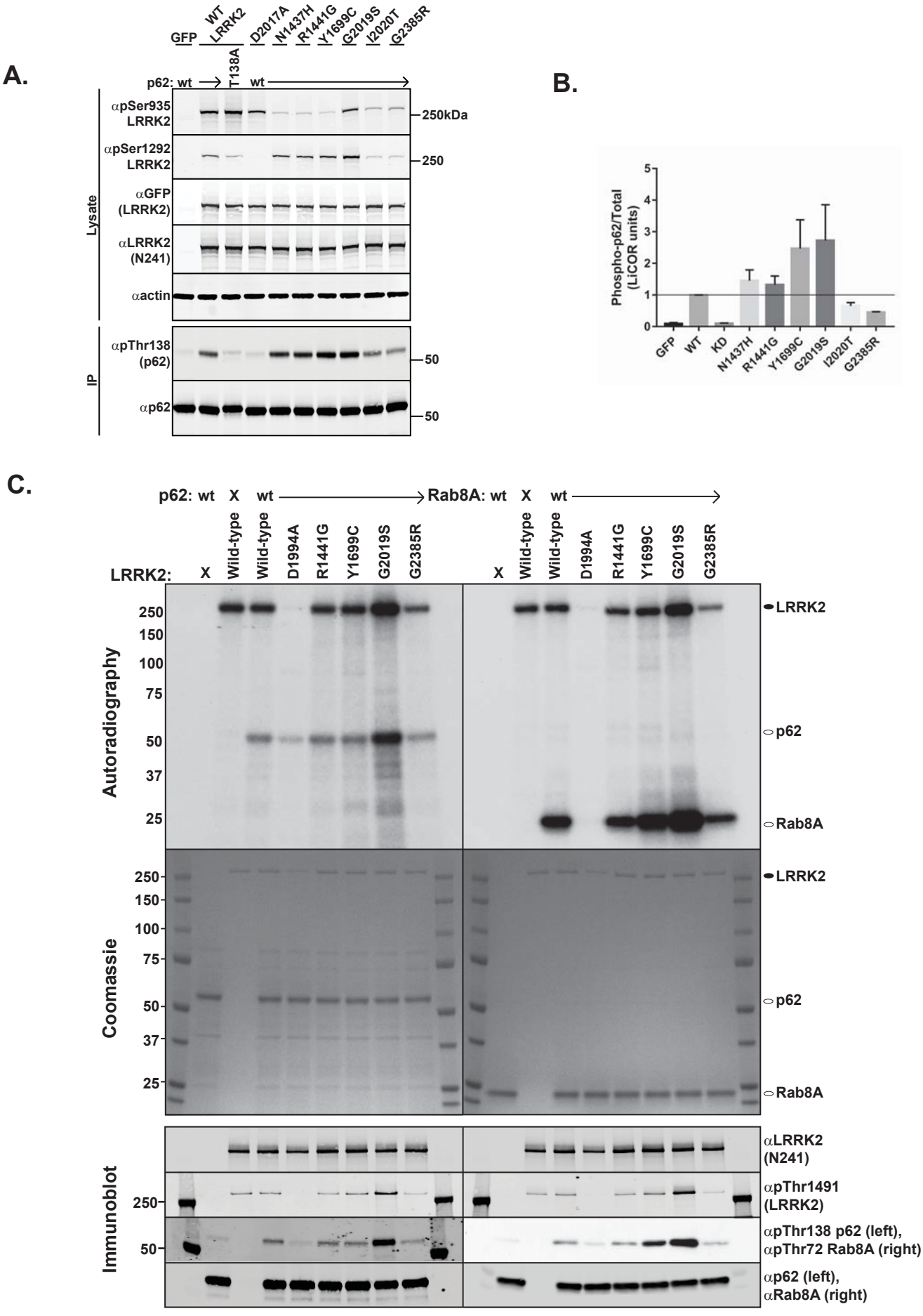
A.
GFP
WT LRRK2
T138A
D2017A
N1437H
R1441G
Y1699C
G2019S
I2020T
G2385R
p62: wt
wt
Lysate
αpSer935 LRRK2
αpSer1292 LRRK2
αGFP (LRRK2)
αLRRK2 (N241)
αactin
IP
αpThr138 (p62)
αp62
250kDa
250
50
50
B.
Phospho-p62/Total (LiCOR units)
GFP
WT
KD
N1437H
R1441G
Y1699C
G2019S
I2020T
G2385R
C.
p62: wt
wt
Rab8A: wt
wt
LRRK2:
X
Wild-type
Wild-type
D1994A
R1441G
Y1699C
G2019S
G2385R
Autoradiography
Coomassie
Immunoblot
LRRK2
p62
Rab8A
αLRRK2 (N241)
αpThr1491 (LRRK2)
αpThr138 p62 (left), αpThr72 Rab8A (right)
αp62 (left), αRab8A (right)

Figure 7

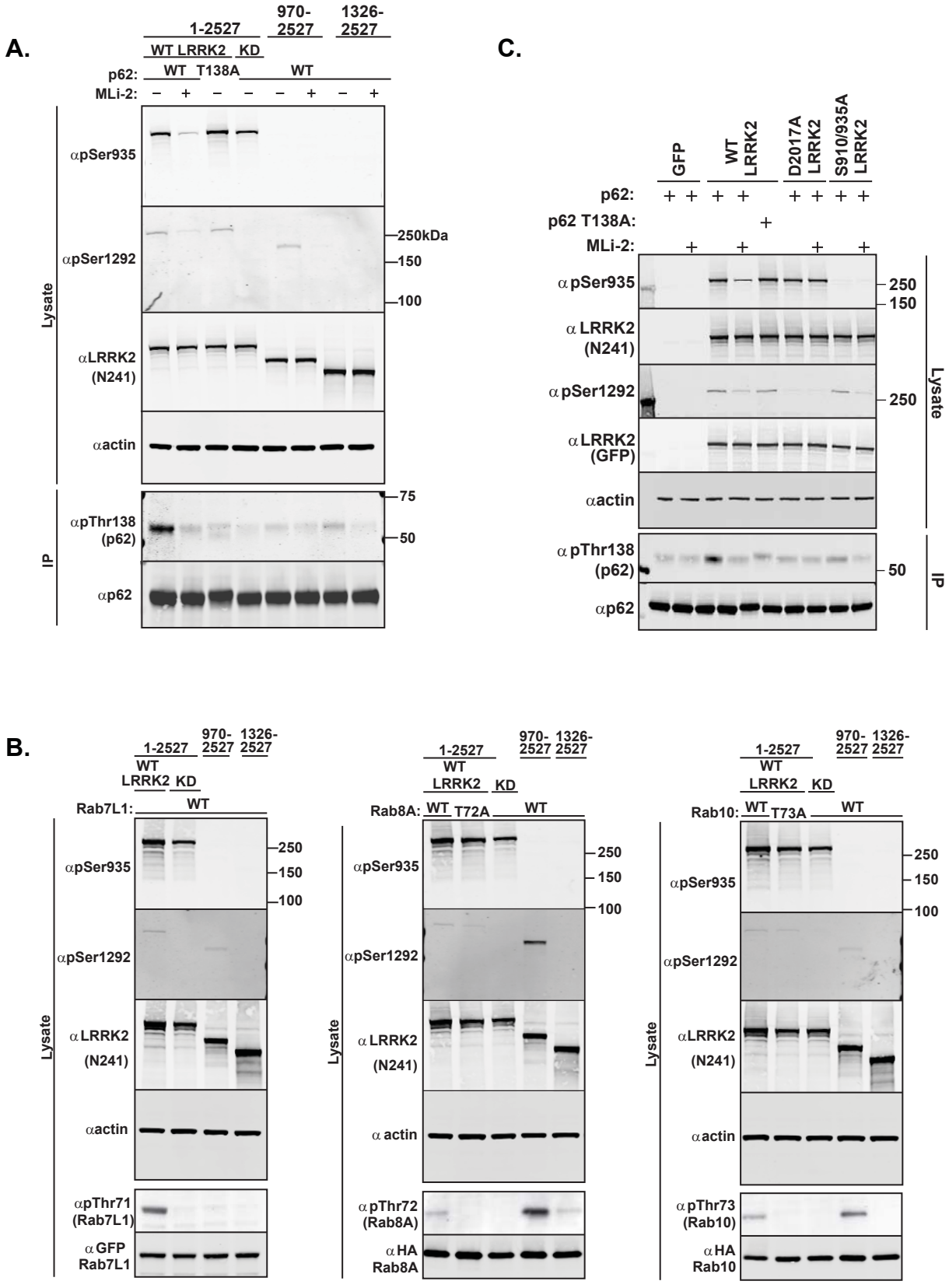
A.
1-2527
970-2527
1326-2527
WT LRRK2
KD
p62:
WT
T138A
WT
MLi-2:
αpSer935
αpSer1292
αLRRK2 (N241)
αactin
Lysate
250kDa
150
100
αpThr138 (p62)
αp62
IP
75
50
B.
Rab7L1:
Rab8A:
T72A
Rab10:
T73A
αpSer935
αpSer1292
αLRRK2 (N241)
αactin
αpThr71 (Rab7L1)
αGFP Rab7L1
αpThr72 (Rab8A)
αHA Rab8A
αpThr73 (Rab10)
αHA Rab10
C.
GFP
WT LRRK2
D2017A LRRK2
S910/935A LRRK2
p62:
p62 T138A:
MLi-2:
αpSer935
αLRRK2 (N241)
αpSer1292
αLRRK2 (GFP)
αactin
αpThr138 (p62)
αp62
250
150
Lysate
IP
50

Figure 8

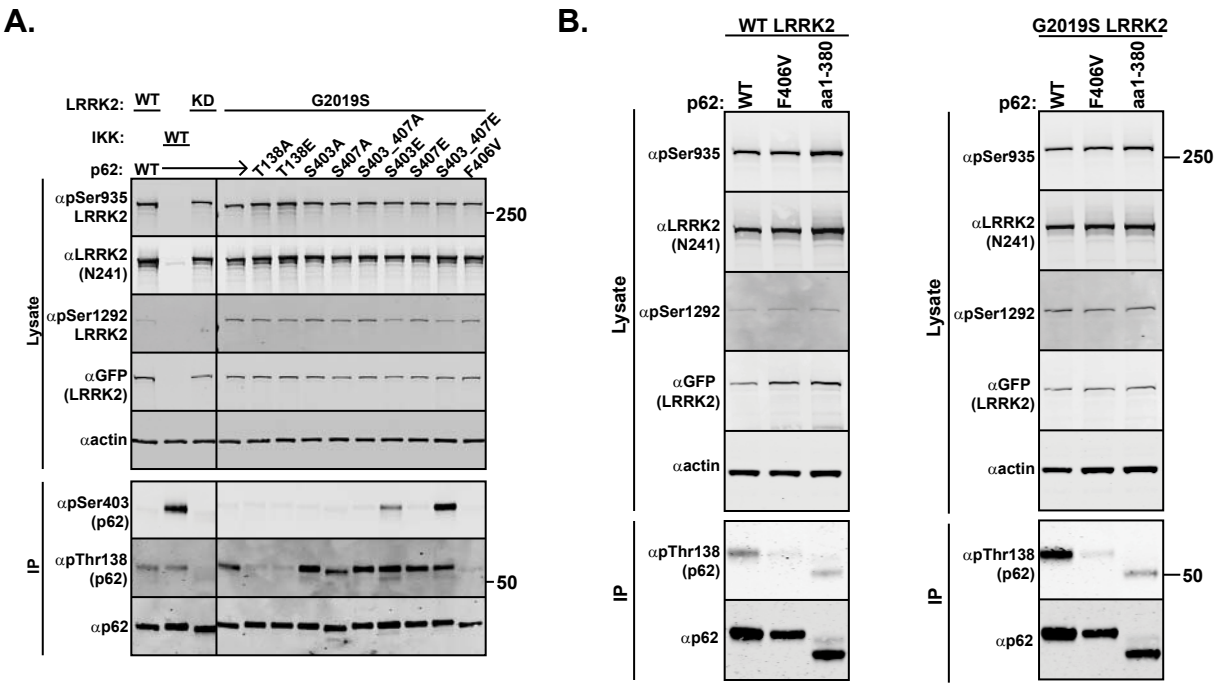
A.
LRRK2: WT KD G2019S
IKK: WT
p62: WT T138A T138E S403A S407A S403_407A S403E S407E S403_407E F406V
Lysate
αpSer935 LRRK2
αLRRK2 (N241)
αpSer1292 LRRK2
αGFP (LRRK2)
αactin
IP
αpSer403 (p62)
αpThr138 (p62)
αp62
250
50
B.
WT LRRK2
G2019S LRRK2
p62: WT F406V aa1-380
Lysate
αpSer935
αLRRK2 (N241)
αpSer1292
αGFP (LRRK2)
αactin
IP
αpThr138 (p62)
αp62
250
50

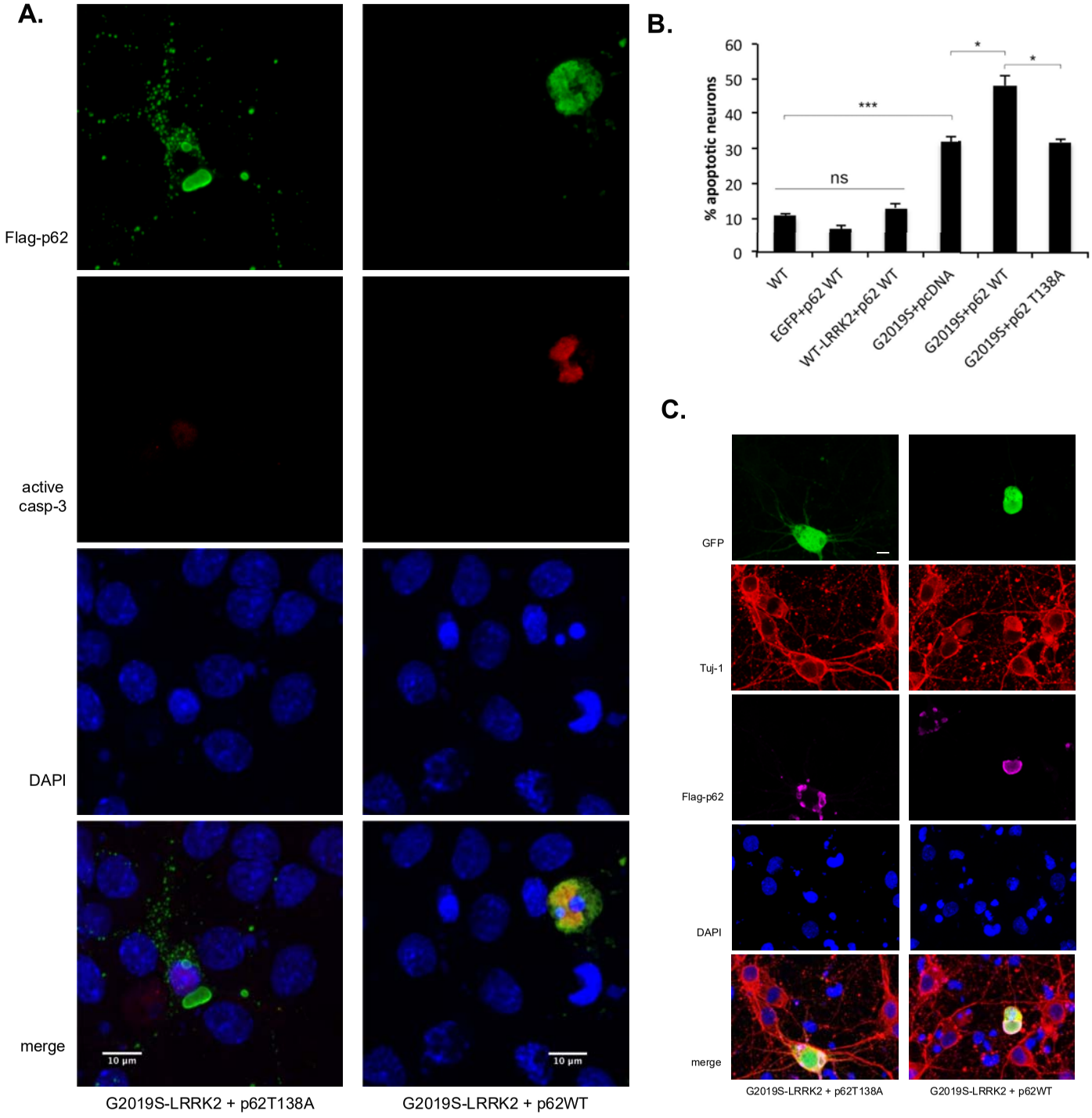
A.
Flag-p62
active casp-3
DAPI
merge
10 µm
10 µm
G2019S-LRRK2 + p62T138A
G2019S-LRRK2 + p62WT
B.
% apoptotic neurons
60
50
40
30
20
10
0
ns
***
*
*
WT
EGFP+p62 WT
WT-LRRK2+p62 WT
G2019S+pcDNA
G2019S+p62 WT
G2019S+p62 T138A
C.
GFP
Tuj-1
Flag-p62
DAPI
merge
G2019S-LRRK2 + p62T138A
G2019S-LRRK2 + p62WT

Supplemental Figure 1

(A)

Generation of CRISPR/Cas9 cell lines. We utilized the CRISPR/Cas9 system to insert eGFP into the endogenous LRRK2 locus of H1299 cells via the homology-directed repair pathway. Three guide sequences with low off-target scores were identified within the LRRK2 start codon region. Complementary oligos with BbsI-compatible overhangs were designed for each target sequence, phosphorylated, annealed to each other, and then ligated into BbsI-digested plasmid pSpCas9(BB)-2A-Puro (PX459) V2.0 (Addgene plasmid #62988), according to (127). As a negative control, we generated a plasmid containing a Scramble sequence (GCACTACCAGAGCTAACTCA). The repair template, described in **(B**, was a 1744 bp DNA fragment consisting of the left homology arm (513 bp of endogenous LRRK2 sequence, ending right after the ATG start codon), followed in-frame by the eGFP sequence, a GGGGS linker, and the right homology arm (another 502 bp of endogenous LRRK2 sequence, beginning after the ATG start codon).

Genomic cleavage detection analysis indicated that the following guide sequence 3 (g*CATG*GCTAGTGGCAGCTGTC, where the initiating methionine is in italics) was most efficient in introducing double-stranded breaks in H1299 cells, and therefore was selected for the generation of the cell line. H1299 cells at ~80% confluency were co-transfected in a six-well plate with 1.25μg CRISPR/Cas9 plasmid (LRRK2 or Scramble) and 1.25μg repair template using Lipofectamine 3000 (Life Technologies), according to the manufacturer's instructions, followed by a 24 h incubation in RPMI-1640 medium supplemented with 10% FBS, 2 mM L-glutamine, 10 mM HEPES, and 1 mM sodium pyruvate. Medium was then replaced with fresh medium supplemented with 8 μg/ml puromycin. After four days of puromycin selection, the medium was replaced again with fresh medium without puromycin. Eight days later cells were dissociated, and single clones were isolated by serial dilutions into 96-well plates (127). After three weeks of expansion, clones were harvested and screened for the presence of GFP by immunoblotting. GFP-positive clones were further analyzed by sequencing. For this purpose, genomic DNA was isolated using the DNeasy Tissue Kit from QIAGEN. PCR was performed using KOD Hot Start DNA Polymerase (Novagen) with primers 5'-CCGCAGGATCCCCGGCTGGCGGGTCGCGG-3' and 5'-GTCAGAGGTTCCTCAAGCCAAATTTTGGG-3' to amplify the target locus (1205 bp fragment amplified on endogenous locus, or 1934 bp fragment amplified on modified locus, shown in (**C**). PCR products were cloned using the Zero Blunt TOPO PCR Cloning Kit for Sequencing (Invitrogen), and individual clones were subjected to sequencing. Note that spectral karyotyping indicated that H1299 cells contain six copies of chromosome 12, on which the human LRRK2 gene is located (128). For biochemical characterization we used a cell line with a 123 bp deletion ending 328 bp upstream of the start codon of the correctly inserted GFP fusion. This clone has at least one modified and one unmodified allele; clone number 4 was utilized in this study.

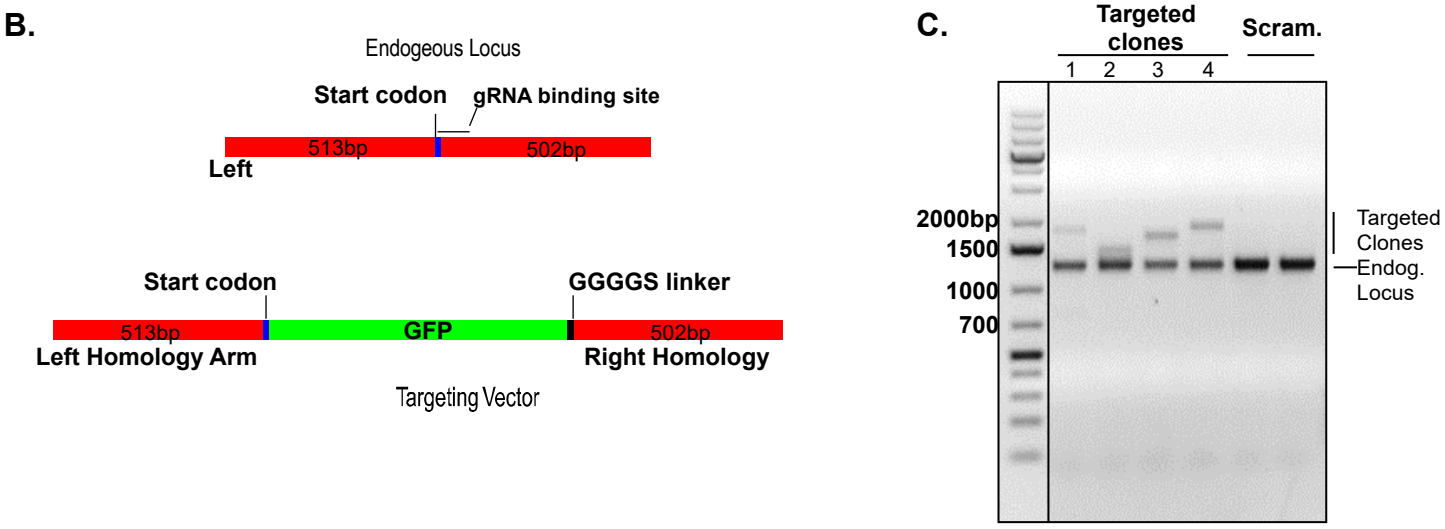

Supplemental Figure 2

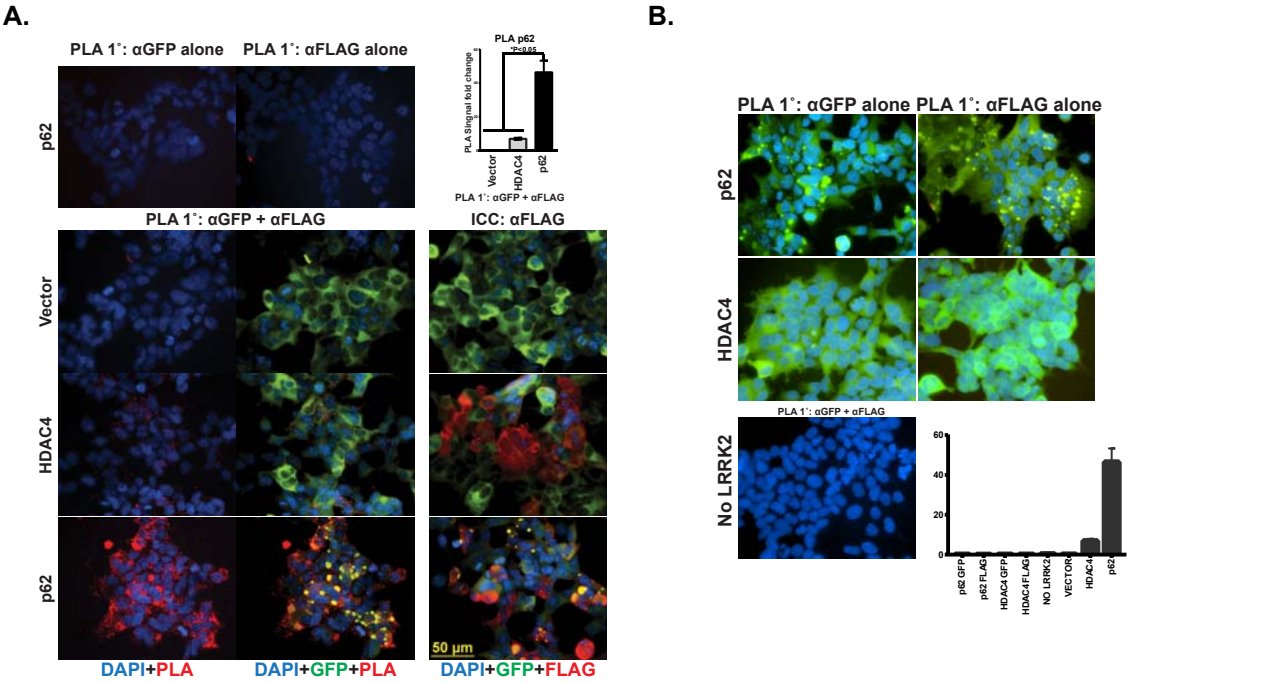

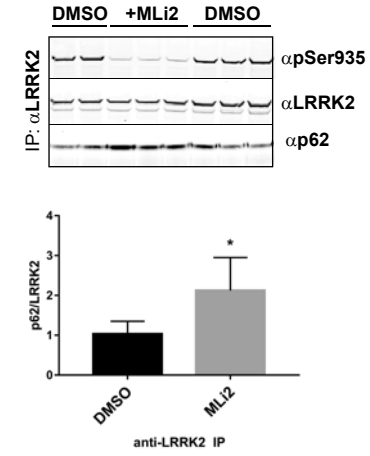

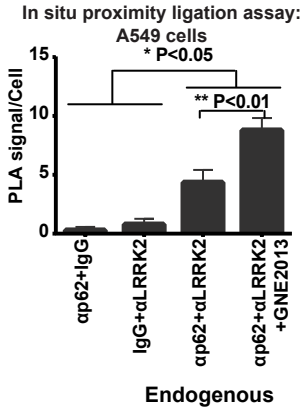

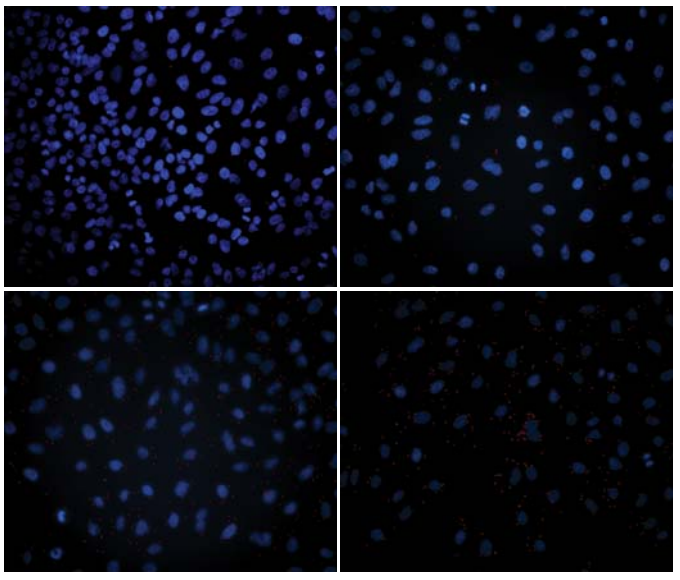

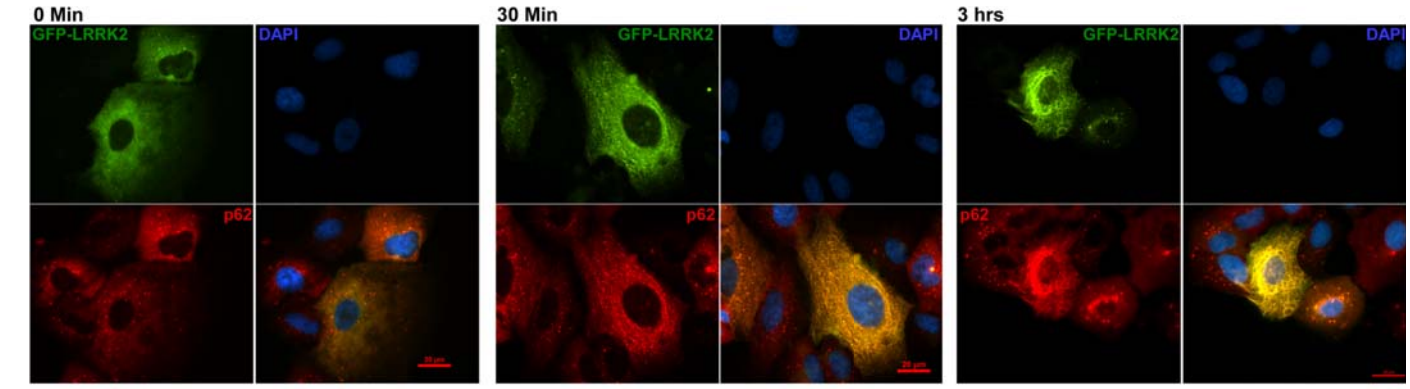

Supplemental Figure 3

A.

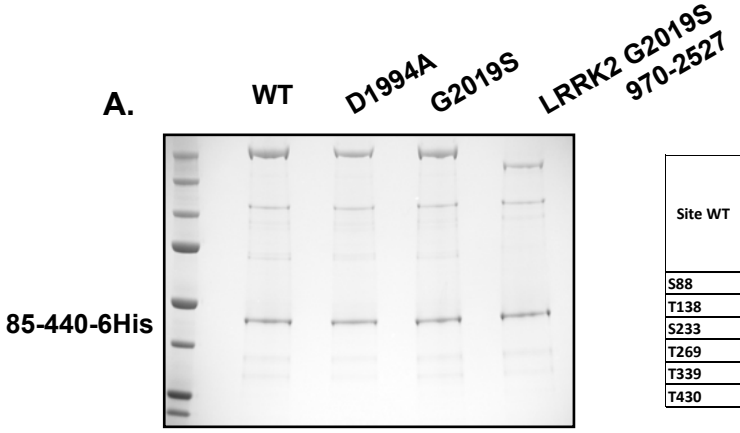

Site WT	Modification	Best Ascore	Localization Probability	LRRK2 (1-2527)	LRRK2 D1994A (1-2527)	LRRK2 G2019S (1-2527)	LRRK2 G2019S (970-2527)
				p62 (85-440)	p62 (85-440)	p62 (85-440)	p62 (85-440)
S88	Phospho	30.97	1	0	0	1	1
T138	Phospho	1,000.00	1	1	0	3	1
S233	Phospho	0	0.5	0	1	0	0
T269	Phospho	15.01	0.97	0	0	1	0
T339	Phospho	0	0.24	0	0	0	1
T430	Phospho	26.2	1	0	0	1	0

B.

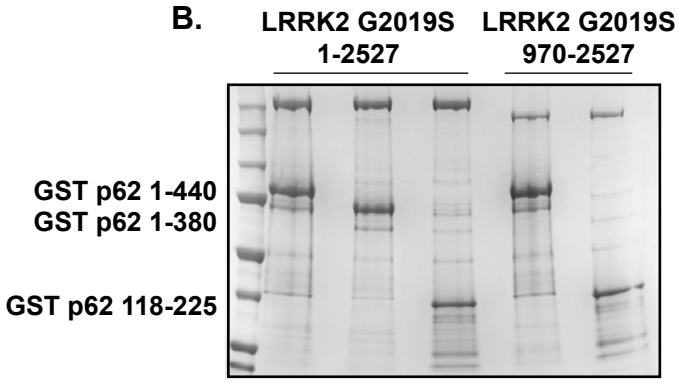

Site WT	Modification	Best Ascore	Localization Probability	LRRK2 G2019S (1-2527)	LRRK2 G2019S (1-2527)	LRRK2 G2019S (1-2527)	LRRK2 G2019S (970-2527)	LRRK2 G2019S (970-2527)
				GST p62 (1-440)	GST-p62 (1-380)	GST-p62 (118-225)	GST-p62 (1-440)	GST-p62 (118-225)
138	Phospho	1,000.00	1	3	5	3	3	2
176	Phospho	1,000.00	1	1	1	0	3	4
180	Phospho	21.95	0.994	0	0	1	0	0
164	Phospho	224.33	1	1	1	1	1	1
269	Phospho	16.24	0.977	2	0	0	0	0
266	Phospho	26.2	0.997	0	0	0	1	0

C.

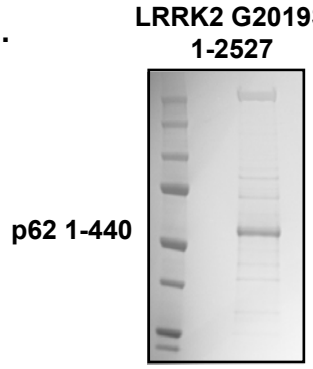

Site WT	Modification	Best Ascore	Localization Probability	LRRK2 (1-2527)
				p62 (1-440)
T138	Phospho	34.46	1	4
T164	Phospho	28.14	1	1
S176	Phospho	132.18	1	1
S182	Phospho	0	0.01	1
S226	Phospho	0	0.33	1
T304	Phospho	148.73	1	1
S306	Phospho	141.12	1	1
Y383	Phospho	56.46	1	1

D.

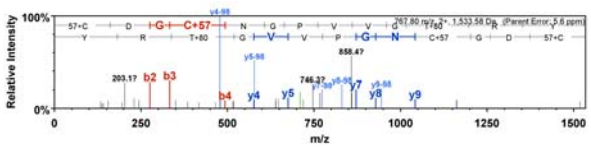

pThr138

E.

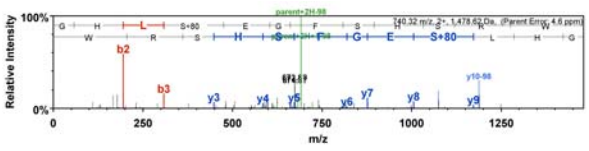

pSer176

F.

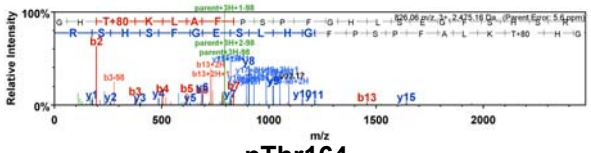

pThr164

Supplementary Figure 4

A.

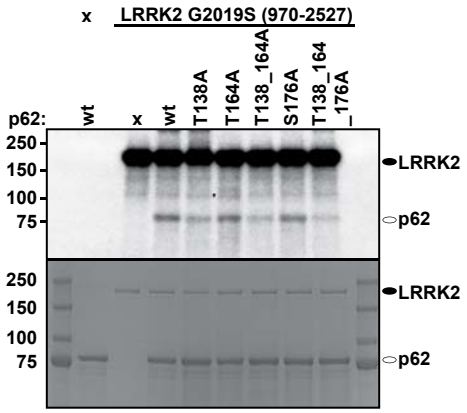

B.

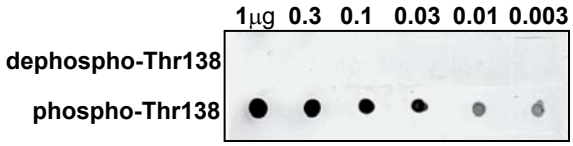

A.

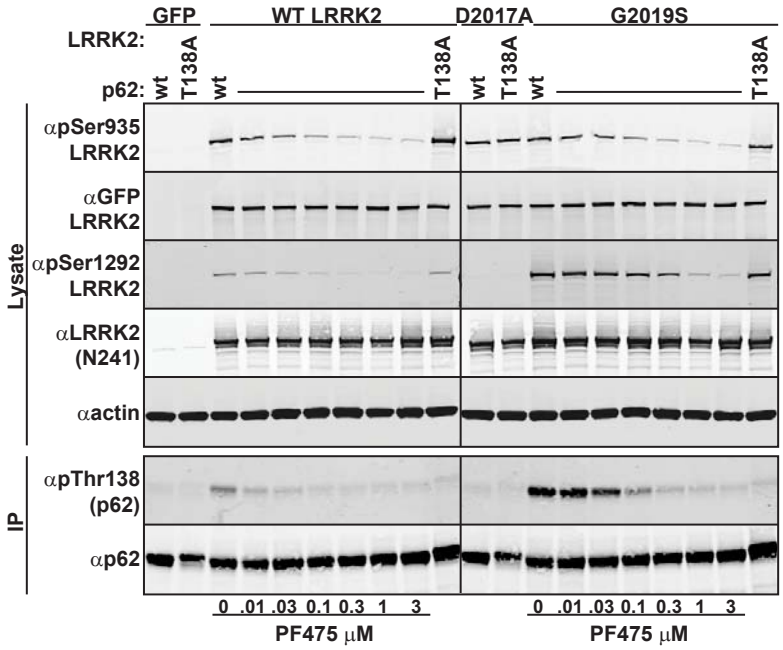
GFP
WT LRRK2
D2017A
G2019S
LRRK2:
p62:
wt
T138A
αpSer935 LRRK2
αGFP LRRK2
αpSer1292 LRRK2
αLRRK2 (N241)
αactin
Lysate
αpThr138 (p62)
αp62
IP
0 .01 .03 0.1 0.3 1 3
PF475 μM

B.

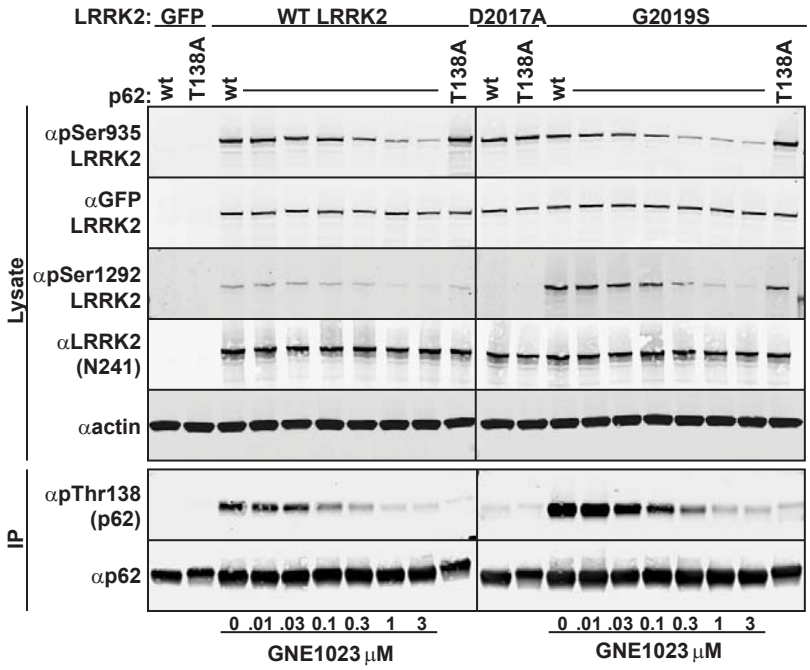
LRRK2: GFP
WT LRRK2
D2017A
G2019S
p62:
wt
T138A
αpSer935 LRRK2
αGFP LRRK2
αpSer1292 LRRK2
αLRRK2 (N241)
αactin
Lysate
αpThr138 (p62)
αp62
IP
0 .01 .03 0.1 0.3 1 3
GNE1023 μM

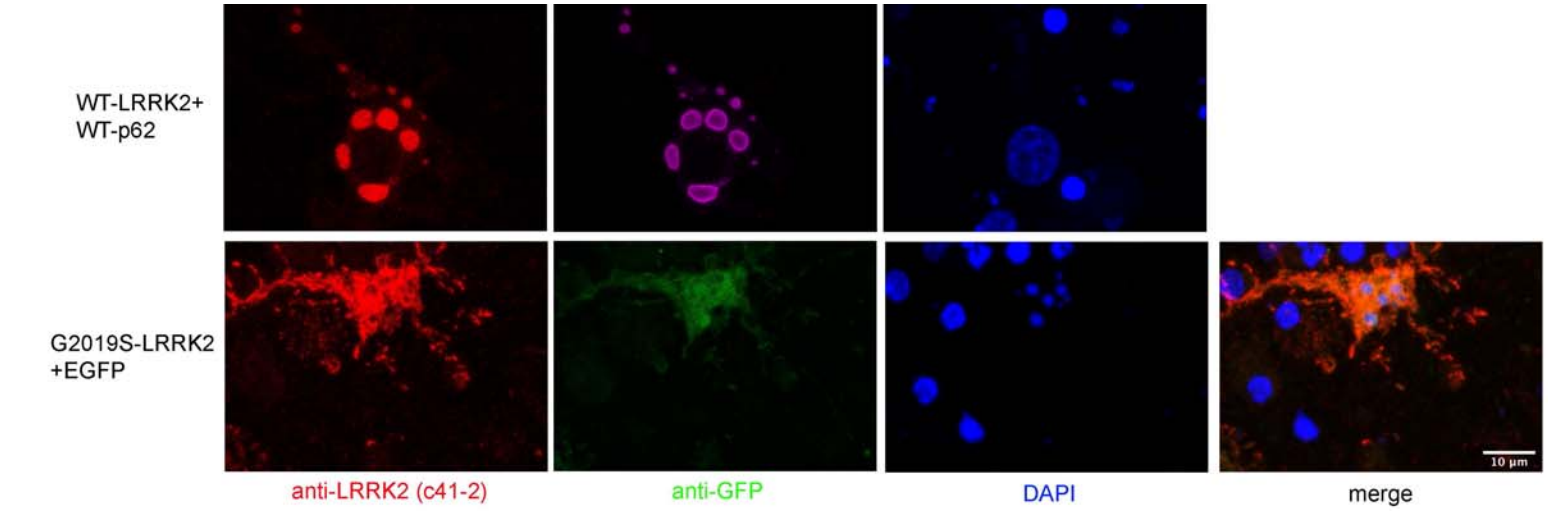
WT-LRRK2+
WT-p62
G2019S-LRRK2
+EGFP
anti-LRRK2 (c41-2)
anti-GFP
DAPI
merge
10 μm

B.

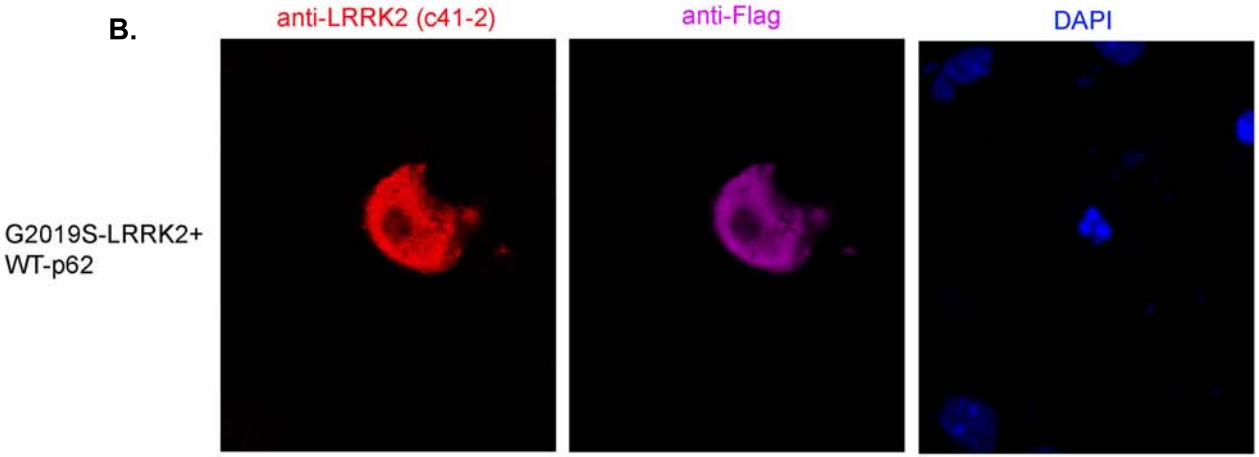
anti-LRRK2 (c41-2)
anti-Flag
DAPI
G2019S-LRRK2+
WT-p62

C.

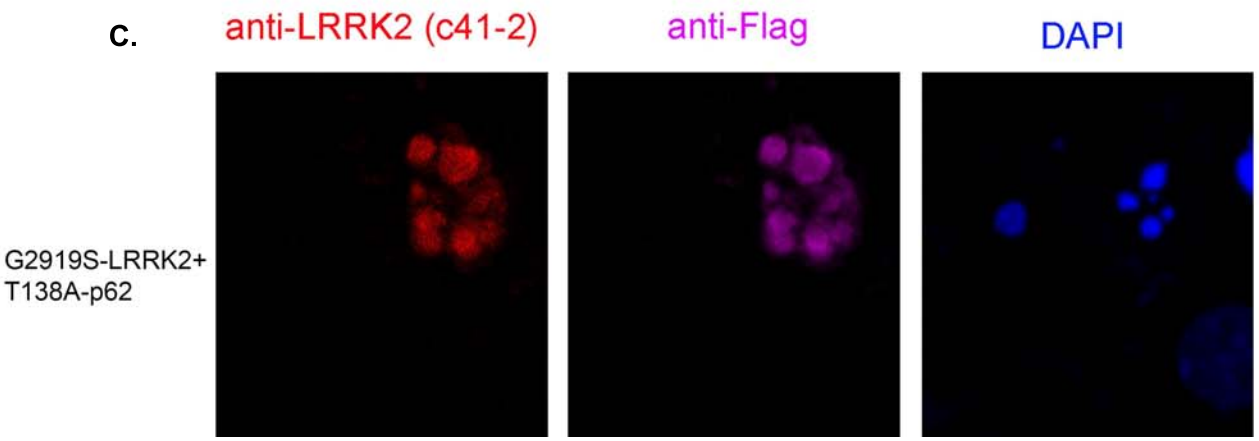
anti-LRRK2 (c41-2)
anti-Flag
DAPI
G2919S-LRRK2+
T138A-p62

Supplemenatal Figure 7